In 2008, mefloquine, an anti-malarial drug, was reported to show activity against JCV *in vitro* [15]. Since then, there have been at least 5 reported cases of PML in which mefloquine was effective [16–20]. In contrast, a recent mefloquine trial of 24 patients with PML (21 HIV-positive and 3 HIV-negative) reported failure in reducing JCV DNA levels in the CSF [21], although it is pending publication. Because there have been no reports describing the details of PML patients demonstrating mefloquine treatment failure, we report two HIV-negative patients with PML in whom mefloquine was not effective.

2. Case reports

2.1. Case 1

A 47-year-old male presented with progressive left hemiparesis. The patient had been treated with chemotherapy including rituximab for Waldenström macroglobulinemia for six years in our hospital. The interval between the last administration of rituximab and occurrence of hemiparesis was about 1 month. Diffusion weighted images (DWI) of brain MRI about 3 months after the onset of hemiparesis demonstrated high intensity areas with internal low intensity areas in the white matter of the right frontal lobe. The apparent diffusion coefficient (ADC) values of the lesion were increased. Because serum IgM had been prominently elevated (around 5000 mg/dl) in association with Waldenström macroglobulinemia, we presumed that the hyperviscosity syndrome resulted in brain infarction.

About 4 months after the onset of hemiparesis, the patient was admitted to our hospital because a convulsion occurred in the left upper and lower limbs. At that time, the patient did not receive any immunosuppressive therapy. On admission, neurological examination revealed upper limb-dominant left hemiparesis, and Babinski's sign and Chaddock's reflex on the left. MRI on admission demonstrated lesion expansion and extension to the right parietal and insular white matter, right putamen, right internal capsule, right thalamus, corpus callosum, left frontal white matter, and midbrain. There was no edema or gadolinium-enhanced lesions. Peripheral blood tests showed white blood cell count (WBC): 3790/μl (normal range: 4500–9000), hemoglobin: 10.4 g/dl (normal range: 13–16), and platelet count: 3.7×10^4/μl (normal range $15–30\times10^4$), indicating pancytopenia. C-reactive protein (CRP) was below 0.1 mg/dl. Testing for HIV was negative. On the next day of admission, a nasogastric feeding tube was inserted because of dysphagia. Four days after admission, CSF examination demonstrated cell count: 1 cell per 3 μl, total protein: 97 mg/dl, and glucose: 67 mg/dl. PCR was positive for JCV DNA in the CSF and detected 1200 copies/ml of DNA. A diagnosis of PML was established based on MRI findings and increased JCV DNA in the CSF.

After diagnosis, the patient developed right hemiparesis and apraxia of speech. Brain MRI 18 days after admission demonstrated lesion expansion and extension to the left insular white matter and left putamen (Fig. 1A). The JCV DNA copy number in the CSF was increased to 4300 copies/ml. $CD4^+$ cell count of the peripheral blood was 219/μl (normal range: 500–1300). Nineteen days after admission, about 5 months after the onset of PML, mefloquine was initiated at a dose of 275 mg/day orally for 3 days, followed by 275 mg once a week [17]. We used Mephaquin Hisamitsu tablets (Hisamitsu Pharmaceutical, Tosu, Japan), which show maximum concentration (C_{max}) of 3.1 μM, time at which C_{max} is observed (T_{max}) of 5.2 h, and terminal half-life (T1/2) of 400.1 h when 1100 mg of drug is once administered. Treatment with mefloquine was approved by the Ethics Committee in our hospital. We obtained written, informed consent from the patient's family. We also used 1 mg/day of risperidone, a 5HT2A receptor blocker at the same time. After initiation of mefloquine, we observed no symptoms suggestive of mefloquine neurotoxicity such as nausea, dizziness, sleep disturbances, anxiety, and psychosis [22]. Eight days after initiation of mefloquine, the JCV DNA copy number in the CSF was increased to 150,000 copies/ml, and the dose of mefloquine was returned to 275 mg/day for 3 days per week (Fig. 2).

However, the JCV DNA copy number in the CSF 22 days after initiation of mefloquine was increased to 850,000 copies/ml. Because of severe aspiration pneumonia, tracheotomy was performed 37 days after initiation of mefloquine. Brain MRI 38 days after initiation of mefloquine demonstrated lesion expansion and extension to the right temporal and occipital white matter and pons (Fig. 1B). The JCV DNA copy number in the CSF 50 days after initiation of mefloquine increased to 3,700,000 copies/ml. Changes in the JCV DNA load are shown in Fig. 2. Brain MRI about 3 months after initiation of mefloquine demonstrated lesion expansion and extension to the left temporal and parietal white matter, left internal capsule, left thalamus, and medulla oblongata (Fig. 1C). The patient died of respiratory failure about 4 months after initiation of mefloquine. The total clinical course of PML was about 9 months. Autopsy could not be performed.

2.2. Case 2

An 81-year-old male with a three-week history of gait disturbance presented with muscle cramp in the bilateral upper limbs and was taken to another hospital by ambulance. Past medical history included hypertension, hyperuricemia, chronic heart failure, and chronic renal failure due to renal sclerosis. A diagnosis of brain infarction of the

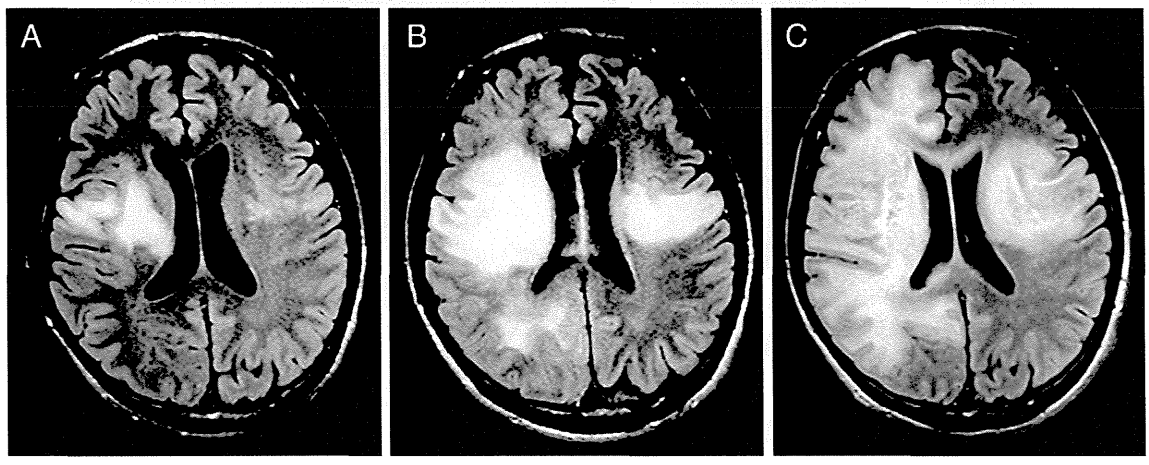

Fig. 1. A. Fluid-attenuated inversion recovery (FLAIR) sequence of brain MRI before initiation of mefloquine demonstrated high intensity areas in the white matter of the bilateral frontal lobes. B, C. FLAIR sequence of brain MRI 38 days (B) and about 3 months (C) after the initiation of mefloquine showed lesion expansion.

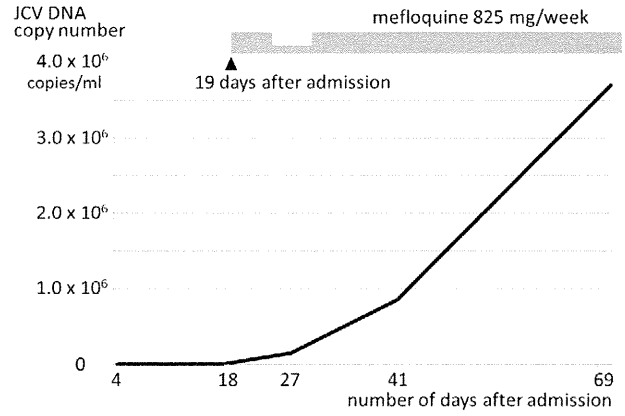

Fig. 2. Changes in the JCV DNA load of case 1 are shown. The JCV DNA copy number in the CSF was increased even after initiation of mefloquine.

subacute phase and the worsening of renal failure was made in the emergency room and the patient was transferred to our hospital.

Physical examination on admission demonstrated muscle cramp in the bilateral upper limbs and face, and right hemiparesis. Consciousness was slightly disturbed, but the orientation to time and place was preserved. Peripheral blood tests showed WBC: 5240/μl, hemoglobin: 7.8 g/dl, platelet count: 17.6×10^4/μl, albumin: 2.7 g/dl (normal range: 3.9–4.9), blood urea nitrogen (BUN): 147 mg/dl (normal range: 8–20), creatinine: 7.83 mg/dl (normal range: 0.6–1.1), creatinine kinase (CK): 445 IU/l (normal range 50–200), CRP: 0.3 mg/dl (normal range <0.1), and glucose: 103 mg/dl. Testing for HIV was negative. Hemodialysis was started on the next day of admission.

DWI of brain MRI 3 days after admission demonstrated high intensity areas in the white matter of the left frontal and parietal lobes and right parietal lobe. ADC values of the lesions were increased. Right hemiparesis progressed after admission, and 18 days after admission, the left hemiparesis emerged. Because of dysphagia, a nasogastric feeding tube was inserted 19 days after admission. CSF examination 20 days after admission demonstrated cell count: 6 cells per 3 μl, total protein: 35 mg/dl, and glucose: 60 mg/dl. PCR was positive for JCV DNA in the CSF, and detected 2223 copies/ml of DNA. A diagnosis of PML was established based on MRI findings and increased JCV DNA in the CSF.

Brain MRI 32 days after admission demonstrated lesion expansion and extension to the corpus callosum and right frontal white matter. Thirty six days after admission, the patient manifested akinetic mutism. Thirty eight days after admission, about 2 months after the onset of PML, mefloquine was initiated at a dose of 275 mg/day orally for 3 days per week. Treatment with mefloquine was approved by the Ethics Committee in our hospital. We obtained written, informed consent from the patient's family. At that time, the JCV DNA copy number in the CSF was increased to 2,790,000 copies/ml. The $CD4^+$ cell count of the peripheral blood was 294/μl. Because whole body CT demonstrated no mass lesions or abnormal lymph node swelling, underlying diseases causing immunodeficiency remained unclear in this patient.

After initiation of mefloquine, we observed no acute neurological deterioration suggesting mefloquine neurotoxicity. Brain MRI 15 days after initiation of mefloquine demonstrated lesion expansion and extension to the bilateral temporal and occipital white matter (Fig. 3A). Twenty nine days after initiation of mefloquine, the JCV DNA copy number in the CSF was increased to 24,075,000 copies/ml. Changes in the JCV DNA load are shown in Fig. 4. Brain MRI 31 days after initiation of mefloquine demonstrated lesion expansion (Fig. 3B). Thirty three days after initiation of mefloquine, hemodialysis was discontinued because of hypotension. The patient died 19 days later. The total clinical course of PML was about 4 months. Autopsy could not be performed.

3. Discussion

Because there is no known specific antiviral agent against JCV, we treated PML in the two HIV-negative patients with mefloquine based on case reports describing the efficacy of mefloquine for PML [16–20]. However, during mefloquine therapy, clinical and radiological progression was observed, and JCV DNA in the CSF was increased in both patients.

Our case 1 had been treated with chemotherapy including rituximab for Waldenström macroglobulinemia. The interval between the last administration of rituximab and diagnosis of PML was about 6 months. Although it is difficult to exclude the possibility that the immunodeficiency due to Waldenström macroglobulinemia itself was related to the occurrence of PML [23], rituximab is well known to cause PML [7]. Rituximab is an anti-CD20 monoclonal antibody that targets human B cells. The pathogenesis of rituximab in PML is considered to decrease B cells in the cerebral perivascular spaces, resulting in decreased antigen presentation to T cells and subsequent alterations in the cellular immune response [7]. One study reported that a median $CD4^+$ cell count was 216/μl in 25 patients who received rituximab [24]. The interval between the last administration of rituximab and

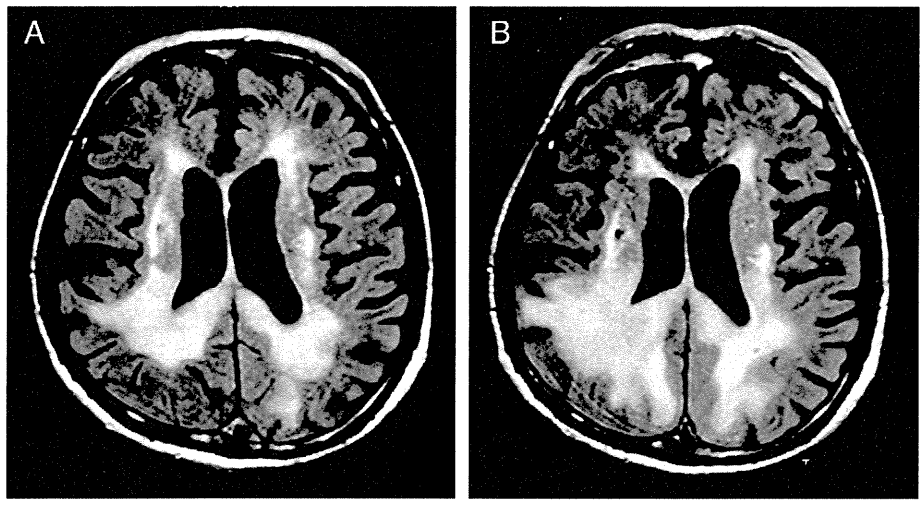

Fig. 3. A. FLAIR sequence of brain MRI 15 days after initiation of mefloquine demonstrated abnormal high intensity areas in the bilateral temporal and occipital white matter. B. FLAIR sequence of brain MRI 31 days after the initiation of mefloquine showed lesion expansion.

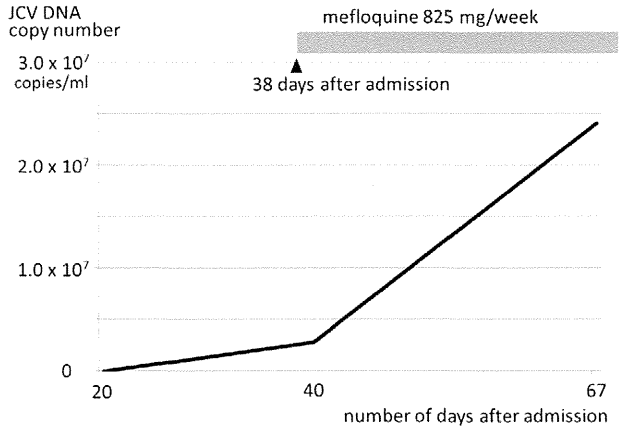

Fig. 4. Changes in the JCV DNA load of case 2 are shown. The JCV DNA copy number in the CSF was increased even after initiation of mefloquine.

diagnosis of PML has been reported to be 5.5 months [25]. Considering that 90% of patients with PML after rituximab therapy die [25], the unfavorable clinical course of our case 1 may be associated with the use of rituximab. In case 2, while $CD4^+$ lymphocytopenia was documented, there were no underlying diseases causing immunodeficiency. However, as PML may occur in patients with minimal or occult immunosuppression [4], idiopathic $CD4^+$ lymphocytopenia may be associated with the occurrence of PML in this patient.

Mefloquine is an anti-malarial drug used both for prophylaxis and treatment of chloroquine resistant *Plasmodium falciparum*. Because mefloquine is highly lipophilic and has a long terminal half-life of more than 1 week [26], a single dose of 15–25 mg/kg is used for treatment and 250 mg/week for prophylaxis. Among subjects administered 250 mg weekly, blood concentrations vary between 1 μM to 5 μM [27]. Mefloquine readily crosses the BBB, where active efflux by the P-glycoprotein membrane transporter prevents its accumulation in the brain [27].

In 2008, mefloquine was reported to show activity against JCV *in vitro* [15]. Brickelmaier et al. showed that mefloquine inhibits viral DNA replication, using quantitative PCR to quantify the number of viral copies in cultured cells. In this study, mefloquine reduced the number of infected cells by 50% or more at a concentration of 3.9 μM [15]. Brickelmaier et al. presumed that efficacious concentrations of mefloquine for PML are achieved in the brains of patients receiving approved doses of the drug [15].

Since the publication by Brickelmaier et al. [15], there have been at least 5 reported cases of PML in which mefloquine was effective [16–20]. The underlying diseases or conditions included sarcoidosis [16], umbilical cord blood transplant [17], HIV infection [18], and systemic lupus erythematosus [19]. $CD4^+$ cell counts in the peripheral blood of patients were described in 3 reports, and were 187/μl [18], 419/μl [17], and 420/μl [16], respectively. JCV DNA loads in the CSF before mefloquine therapy were available in these reports, and were 33,700 copies/ml [16], 535,500 copies/ml [18], and 911,175 copies/ml [17], respectively. The intervals between symptom onset and initiation of mefloquine therapy were about 3 months [17,19], 5 months [18], and 6 months [16,20], respectively. In 4 reports [16–19], the authors stated that PCR for JCV in the CSF became negative after mefloquine therapy. At present, the patients' background or laboratory data common among these cases showing responses to mefloquine therapy is unclear.

In contrast to these cases, a recent mefloquine trial of 24 patients with PML (21 HIV-positive and 3 HIV-negative) reported failure in reducing JCV DNA levels in the CSF [21]. Participants took 250 mg of mefloquine 4 times daily, followed by 250 mg weekly. The failure of this trial and the poor outcome of our patients raise the possibility that the improvement observed in mefloquine therapy in reported PML patients [16–20] may actually reflect the natural favorable course of those patients.

At present, we cannot tell the difference in patient backgrounds or laboratory data between patients showing responses to mefloquine [16–20] and our patients. Regarding the presence of both mefloquine responders and non-responders in PML, Nevin stated that responses to mefloquine may correlate with polymorphisms in the *MDR1* gene coding for P-glycoprotein that affect drug efflux across the BBB [28]. In cases of unsuccessful treatment of PML, active efflux as a result of drug induced upregulation of P-glycoprotein expression in the BBB may be preventing therapeutic concentrations of mefloquine [28]. From this point of view, co-administration of P-glycoprotein inhibitors or substrates such as risperidone may be recommended in the treatment of PML [27]. On the other hand, considering the failure of the mefloquine trial and the poor outcome of our patients, re-evaluation of the anti-JCV activity of mefloquine may be required. If the anti-JCV activity of mefloquine is verified again, further studies are necessary to clarify whether the response to mefloquine in PML is influenced by the presence of HIV infection, $CD4^+$ cell counts, JCV DNA levels in the CSF, blood concentration of mefloquine, interval between disease onset and initiation of therapy, or *MDR1* polymorphism.

Conflict of interest statement

The authors have no conflicts of interest.

Acknowledgment

The authors thank Dr. Takayoshi Ito, Tamaki Kuyama, and Yuji Nakamura for clinical management of the patients. The study was financially supported by a grants-in-aid from the Research Committee of Prion Disease and Slow Virus Infection (H20-Nanchi-Ippan-013) and by those for Scientific Research from the Ministry of Education, Science, Sports and Culture of Japan (19790349 and 22790446), and by those for Research on HIV/AIDS (H24-AIDS-Wakate-002) from the Ministry of Health, Labour and Welfare of Japan.

References

[1] Marzocchetti A, Tompkins T, Clifford DB, Gandhi RT, Kesari S, Berger JR, et al. Determinants of survival in progressive multifocal leukoencephalopathy. Neurology 2009;73:1551-8.
[2] Shishido-Hara Y. Progressive multifocal leukoencephalopathy and promyelocytic leukemia nuclear bodies: a review of clinical, neuropathological, and virological aspects of JC virus-induced demyelinating disease. Acta Neuropathol 2010;120:403-17.
[3] Molloy ES, Calabrese LH. Progressive multifocal leukoencephalopathy: a national estimate of frequency in systemic lupus erythematosus and other rheumatic diseases. Arthritis Rheum 2009;60:3761-5.
[4] Gheuens S, Pierone G, Peeters P, Koralnik IJ. Progressive multifocal leukoencephalopathy in individuals with minimal or occult immunosuppression. J Neurol Neurosurg Psychiatry 2010;81:247-54.
[5] Kishida S. Progressive multifocal leukoencephalopathy—epidemiology, clinical pictures, diagnosis and therapy. Brain Nerve 2007;59:125-37.
[6] Mizusawa H, Kishida S, Saijo M, Yukishita M, Shishido-Hara Y, Sawa H, et al. Progressive multifocal leukoencephalopathy (PML). Rinsho Shinkeigaku 2011;51:1051-7.
[7] Tan CS, Koralnik IJ. Progressive multifocal leukoencephalopathy and other disorders caused by JC virus: clinical features and pathogenesis. Lancet Neurol 2010;9:425-37.
[8] Rueger MA, Miletic H, Dorries K, Wyen C, Eggers C, Deckert M, et al. Long-term remission in progressive multifocal leukoencephalopathy caused by idiopathic CD4+ T lymphocytopenia: a case report. Clin Infect Dis 2006;42:e53-6.
[9] Bossolasco S, Calori G, Moretti F, Boschini A, Bertelli D, Mena M, et al. Prognostic significance of JC virus DNA levels in cerebrospinal fluid of patients with HIV-associated progressive multifocal leukoencephalopathy. Clin Infect Dis 2005;40:738-44.
[10] Andrei G, Snoeck R, Vandeputte M, De Clercq E. Activities of various compounds against murine and primate polyomaviruses. Antimicrob Agents Chemother 1997;41:587-93.
[11] Hou J, Major EO. The efficacy of nucleoside analogs against JC virus multiplication in a persistently infected human fetal brain cell line. J Neurovirol 1998;4:451-6.
[12] Hall CD, Dafni U, Simpson D, Clifford D, Wetherill PE, Cohen B, et al. Failure of cytarabine in progressive multifocal leukoencephalopathy associated with human

immunodeficiency virus infection. AIDS Clinical Trials Group 243 Team. N Engl J Med 1998;338:1345-51.
[13] Marra CM, Rajicic N, Barker DE, Cohen BA, Clifford D, Donovan Post MJ, et al. A pilot study of cidofovir for progressive multifocal leukoencephalopathy in AIDS. AIDS 2002;16:1791-7.
[14] Wyen C, Hoffmann C, Schmeisser N, Wöhrmann A, Qurishi N, Rockstroh J, et al. Progressive multifocal leukencephalopathy in patients on highly active antiretroviral therapy: survival and risk factors of death. J Acquir Immune Defic Syndr 2004;37: 1263-8.
[15] Brickelmaier M, Lugovskoy A, Kartikeyan R, Reviriego-Mendoza MM, Allaire N, Simon K, et al. Identification and characterization of mefloquine efficacy against JC virus *in vitro*. Antimicrob Agents Chemother 2009;53:1840-9.
[16] Gofton TE, Al-Khotani A, O'Farrell B, Ang LC, McLachlan RS. Mefloquine in the treatment of progressive multifocal leukoencephalopathy. J Neurol Neurosurg Psychiatry 2011;82:452-5.
[17] Kishida S, Tanaka K. Mefloquine treatment in a patient suffering from progressive multifocal leukoencephalopathy after umbilical cord blood transplant. Intern Med 2010;49:2509-13.
[18] Naito K, Ueno H, Sekine M, Kanemitsu M, Ohshita T, Nakamura T, et al. Akinetic mutism caused by HIV-associated progressive multifocal leukoencephalopathy was successfully treated with mefloquine: a serial multimodal MRI study. Intern Med 2012;51:205-9.
[19] Beppu M, Kawamoto M, Nukuzuma S, Kohara N. Mefloquine improved progressive multifocal leukoencephalopathy in a patient with systemic lupus erythematosus. Intern Med 2012;51:1245-7.
[20] Hirayama M, Nosaki Y, Matsui K, Terao S, Kuwayama M, Tateyama H, et al. Efficacy of mefloquine to progressive multifocal leukoencephalopathy initially presented with parkinsonism. Clin Neurol Neurosurg 2012;114:728-31.
[21] Friedman R. News from the AAN Annual Meeting: malaria drug fails to fulfill promise in PML. Neurol Today 2011;11:8.
[22] Toovey S. Mefloquine neurotoxicity: a literature review. Travel Med Infect Dis 2009;7:2-6.
[23] Chiarchiaro J, McLendon RE, Buckley PJ, Laskowitz DT. Progressive multifocal leukoencephalopathy with occult Waldenström macroglobulinemia. J Clin Oncol 2010;28:e759-61.
[24] Laszlo D, Bassi S, Andreola G, Agazzi A, Antoniotti P, Balzano R, et al. Peripheral T-lymphocyte subsets in patients treated with rituximab–chlorambucil combination therapy for indolent NHL. Ann Hematol 2006;85:813-4.
[25] Carson KR, Evens AM, Richey EA, Habermann TM, Focosi D, Seymour JF, et al. Progressive multifocal leukoencephalopathy after rituximab therapy in HIV-negative patients: a report of 57 cases from the Research on Adverse Drug Events and Reports project. Blood 2009;113:4834-40.
[26] Looareesuwan S, White NJ, Warrell DA, Forgo I, Dubach UG, Ranalder UB, et al. Studies of mefloquine bioavailability and kinetics using a stable isotope technique: a comparison of Thai patients with falciparum malaria and healthy Caucasian volunteers. Br J Clin Pharmacol 1987;24:37-42.
[27] Nevin RL. Pharmacokinetic considerations in the repositioning of mefloquine for treatment of progressive multifocal leukoencephalopathy. Clin Neurol Neurosurg 2012;114:1204-5.
[28] Nevin RL. Neuropharmacokinetic heterogeneity of mefloquine in the treatment of progressive multifocal leukoencephalopathy. Intern Med 2012;51:2257.

blood

2013 121: 4512-4520
Prepublished online March 25, 2013;
doi:10.1182/blood-2012-08-450494

EZH2 overexpression in natural killer/T-cell lymphoma confers growth advantage independently of histone methyltransferase activity

Junli Yan, Siok-Bian Ng, Jim Liang-Seah Tay, Baohong Lin, Tze Loong Koh, Joy Tan, Viknesvaran Selvarajan, Shaw-Cheng Liu, Chonglei Bi, Shi Wang, Shoa-Nian Choo, Norio Shimizu, Gaofeng Huang, Qiang Yu and Wee-Joo Chng

Blood (print ISSN 0006-4971, online ISSN 1528-0020), is published weekly by the American Society of Hematology, 2021 L St, NW, Suite 900, Washington DC 20036.

Regular Article

LYMPHOID NEOPLASIA

EZH2 overexpression in natural killer/T-cell lymphoma confers growth advantage independently of histone methyltransferase activity

Junli Yan,[1] Siok-Bian Ng,[1-3] Jim Liang-Seah Tay,[3] Baohong Lin,[4] Tze Loong Koh,[4] Joy Tan,[3] Viknesvaran Selvarajan,[2,3] Shaw-Cheng Liu,[1] Chonglei Bi,[1] Shi Wang,[2] Shoa-Nian Choo,[2,3] Norio Shimizu,[5] Gaofeng Huang,[1] Qiang Yu,[6] and Wee-Joo Chng[1,3,4]

[1]Cancer Science Institute of Singapore, National University of Singapore, Singapore; [2]Department of Pathology, National University Health System, Singapore; [3]Yong Loo Lin School of Medicine, National University of Singapore, Singapore; [4]Department of Haematology-Oncology, National University Cancer Institute of Singapore, National University Health System, Singapore; [5]Department of Virology, Tokyo Medical and Dental University, Tokyo, Japan; and [6]Department of Cancer Biology and Pharmacology, Genome Institute of Singapore, Agency for Science, Technology and Research, Biopolis, Singapore

Key Points

- This study has uncovered an oncogenic role of EZH2 independent of its methyltransferase activity in NKTL.
- This study suggests that targeting EZH2 may have therapeutic usefulness in NKTL.

The role of enhancer of zeste homolog 2 (EZH2) in cancer is complex and may vary depending on the cellular context. We found that EZH2 is aberrantly overexpressed in the majority of natural killer/T-cell lymphoma (NKTL), an aggressive lymphoid malignancy with very poor prognosis. We show that EZH2 upregulation is mediated by MYC-induced repression of its regulatory micro RNAs and EZH2 exerts oncogenic properties in NKTL. Ectopic expression of EZH2 in both primary NK cells and NKTL cell lines leads to a significant growth advantage. Conversely, knock-down of EZH2 in NKTL cell lines results in cell growth inhibition. Intriguingly, ectopic EZH2 mutant deficient for histone methyltransferase activity is also able to confer growth advantage and rescue growth inhibition on endogenous EZH2 depletion in NKTL cells, indicating an oncogenic role of EZH2 independent of its gene-silencing activity. Mechanistically, we show that EZH2 directly promotes the transcription of cyclin D1 and this effect is independent of its enzymatic activity. Furthermore, depletion of EZH2 using a PRC2 inhibitor 3-deazaneplanocin A significantly inhibits growth of NK tumor cells. Therefore, our study uncovers an oncogenic role of EZH2 independent of its methyltransferase activity in NKTL and suggests that targeting EZH2 may have therapeutic usefulness in this lymphoma. (*Blood.* 2013;121(22):4512-4520)

Introduction

Nasal-type natural killer/T-cell lymphoma (NKTL) is an aggressive lymphoid malignancy associated with very poor survival outcomes.[1] A better understanding of the molecular abnormalities underlying this disease will provide important insights into the biology of this tumor; however, studies on NKTL are often limited by the lack of adequate tissue in small nasal biopsies and the presence of necrosis in biopsy specimens. Although more effective therapy is now available, treatment is still completely reliant on radiotherapy and combinations of chemotherapy.[2,3]

We and others have recently performed whole-genome gene expression studies and identify a number of genes that are differentially expressed in NKTL as well as pathways that are activated in NKTL. Enhancer of zeste homolog 2 (EZH2), one of the genes identified in our study to be aberrantly overexpressed in NKTL,[4] is a H3K27-specific histone methyltransferase and a component of the polycomb repressive complex 2 (PRC2), which plays a key role in the epigenetic maintenance of repressive chromatin mark. EZH2 protein contains a catalytic domain (SET domain) at the COOH-terminus that provides the methyltransferase activity. The catalytic domain must partner with other noncatalytic proteins, such as EED and SUZ12, to form the PRC2 in order to attain robust histone methyltransferase activity. Genome-wide approaches have demonstrated the importance of the PRC2 complex in the transcriptional regulation through H3K27 methylation and gene repression.[5]

Published literature reveals a number of possible mechanisms of EZH2 upregulation in different types of human cancers.[6] It has been shown that EZH2 expression can be transcriptionally activated by a fusion oncoprotein EWS-FLI1 in Ewing sarcoma.[7] EZH2 expression in the breast tumor–initiating cell population is particularly enhanced by hypoxia through HIF1a-mediated transactivation.[8] In addition to transcriptional regulation, the EZH2 transcript is known to be regulated by tumor suppressor micro RNAs (miRNAs). For example, miR-26a binds to and inhibits EZH2 transcript expression in B-cell lymphoma.[9] miR-101 is frequently lost in metastatic prostate cancer, thus releasing EZH2 from miR-101–mediated repression.[10] EZH2 can also be modulated by post-translational modifications through

Submitted August 16, 2012; accepted March 19, 2013. Prepublished online as *Blood* First Edition paper, March 25, 2013; DOI 10.1182/blood-2012-08-450494.

J.Y. and S.-B.N. contributed equally to this study.

The online version of this article contains a data supplement.

The publication costs of this article were defrayed in part by page charge payment. Therefore, and solely to indicate this fact, this article is hereby marked "advertisement" in accordance with 18 USC section 1734.

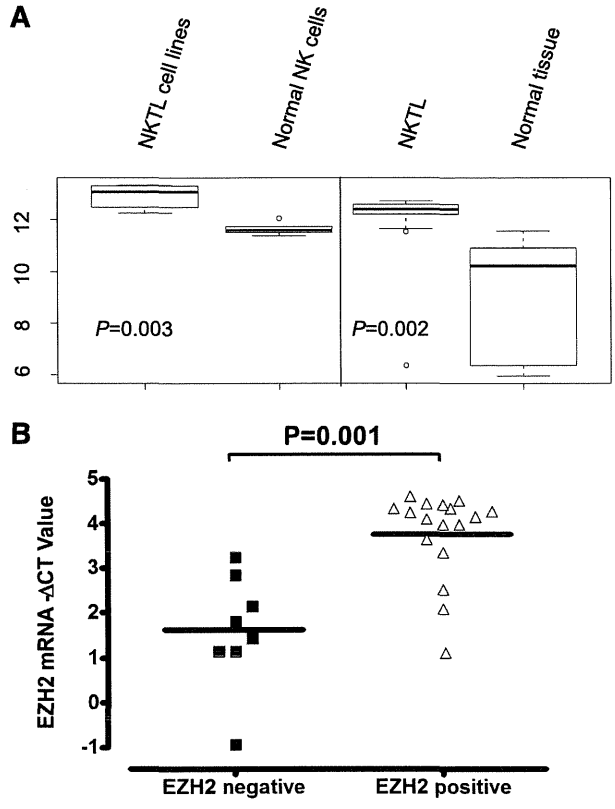

Figure 1. EZH2 mRNA levels are elevated in NKTL and cell lines. (A) Expression score for EZH2 mRNAs in NKTL GEP dataset. EZH2 gene expressions in NKTL FFPE samples were compared with that in respective normal FFPE tissue controls, as well as the NK cell lines and normal NK cells using significance analysis of microarray. (B) Correlation between EZH2 transcript levels determined by qRT-PCR and EZH2 protein levels measured by IHC for NKTL samples.

phosphorylation by AKT and cyclin-dependent kinase.[11,12] To the best of our knowledge, the mechanism of EZH2 overexpression in NKTL has not yet been described.

A high level of EZH2 expression is associated with aggressiveness and poor outcome in solid tumors such as prostate, breast, and endometrial cancers. The oncogenic role of EZH2 overexpression in these tumor types has been studied extensively. In human B-cell malignancies, mutations of Y641 and A677 have been documented to be associated with profoundly increased activity for methylated H3K27, which may promote the development of lymphoma.[13-15] On the other hand, recent discoveries of recurrent somatic *EZH2* mutations in myelodysplastic syndromes and myeloproliferative neoplasms indicate that inactivation of EZH2 may contribute to the pathogenesis of myeloid malignancies.[16,17] Genetic inactivation of EZH2 has also been identified in T-cell acute lymphoblastic leukemia, and the study by Ntziachristos and colleagues suggests a tumor suppressor role for EZH2 in human leukemia by a hitherto unrecognized dynamic interplay between oncogenic NOTCH1 and EZH2.[18] Taken together, the role of EZH2 and the underlying mechanisms of gene regulation by EZH2 in cancer are complex, and further studies need to be performed in a cell context–dependent manner.

In our study, we demonstrated the overexpression of EZH2 in NKTL, deciphered the molecular mechanisms underlying the overabundance of EZH2, and investigated its functional role as an oncogene in this disease. Contrary to our expectations, we found that EZH2 overexpression is not associated with H3K27 trimethylation in NKTL, and its oncogenic activity does not require its histone methyltransferase activity. Instead, EZH2 directly promotes cyclin D1 expression. Thus, this study demonstrates a noncanonic role of EZH2 in NKTL.

Methods

Immunohistochemistry

A total of 38 clinical cases of NKTL that fulfill the World Health Organization diagnostic criteria were used for immunohistochemistry (IHC) studies. The clinicopathologic data of the cases are included in supplemental Table 1. There were 27 cases that came from the tissue microarray used in our previous study (GEO accession no. GSE31377).[4] IHC analysis was performed for EZH2, Ki67, and H3K27me3 on 4-μm sections of NKTL using the conditions listed in supplemental Table 2. IHC study was also performed on cell blocks of normal NK cells for comparison. Appropriate positive tissue controls were used. Details of scoring and imaging are appended in the supplemental Methods.

Primary NK cell isolation and retroviral transduction

Highly purified (90%-99%) normal human NK cells were isolated and cultured as described previously.[19] Retroviruses were generated by transfection of empty plasmid vector polymorphonuclear neutrophil (pMN)-enhanced green fluorescence protein (EGFP) or vectors containing EZH2 using Fugene HD6 into Phoenix-amphotropic packaging cells. At 48 hours after transfection, the supernatants were collected and filtered. A total of 200 000 cells were mixed with 1.6 mL of retroviral supernatant in 12-well plates with 10 μg/mL of Polybrene added. The infection was repeated at 72 hours after transfection.

Luciferase reporter assay

The cyclin D1 (CCND1) promoter construct pGL4-CCND1-Luc has been described previously.[20] Cells were harvested 24 hours after transfection and were analyzed with the Dual Luciferase system (Promega). See the supplemental Methods and Materials for details.

ChIP assay

Chromatin immunoprecipitation (ChIP) assays were performed as described previously.[21] See the supplemental Methods and Materials for details of the antibodies used and primer sequences.

Western blotting

Cells were lysed in radioimmunoprecipitation assay buffer and were subjected to sonication. The primary antibodies used included cell-signaling antibody EZH2 (4905), H3K27me3 (07-449), H3K27me2 (9755), Total H3 (9715) and SantaCruz antibody CCND1 (DCS-6 and A12), and cleaved poly (ADP-ribose)polymerase (PARP; F2, sc-8007).

Full methods are provided in the supplemental information.

Results

EZH2 is overexpressed in NKTL

In our previously published genome-wide gene expression profiling (GEP) of extranodal nasal-type NKTL,[4] the EZH2 transcript level was significantly higher in NKTL compared with normal NK cells (Figure 1A). In corroboration with the GEP findings, we observed a significant percentage of cases (61%) showing positive expression of EZH2 protein in the tumor cells in our 38 cases of NKTL (tissue microarrays or whole-tissue sections) by IHC studies (supplemental Figure 1; supplemental Table 3), whereas the normal NK cells only showed a minimal level of EZH2 (staining in ≤5% cells). Indeed,

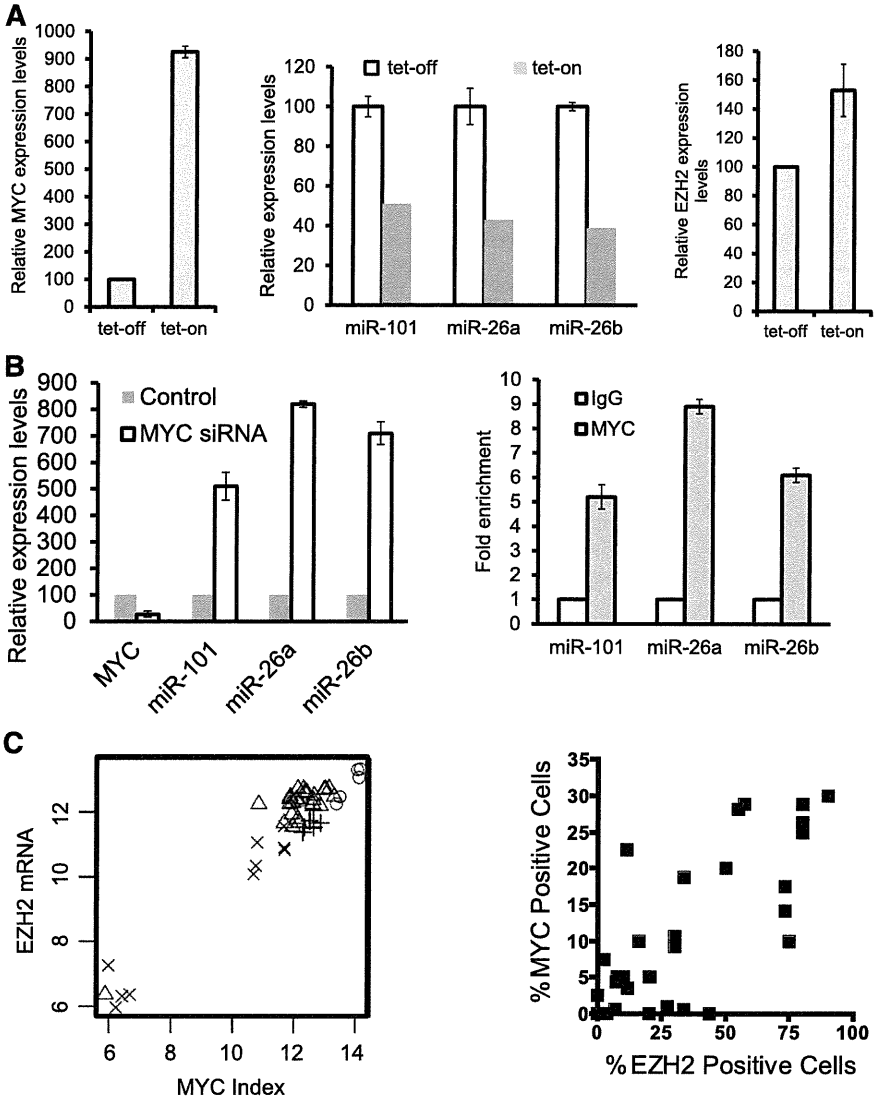

Figure 2. Inhibition of EZH2 expression by miRNA-101 and miRNA-26, which are suppressed by MYC in NKTL cells. (A, left) MYC induction by tet-on. MYC overexpression was induced by treating cells with doxycycline. MYC expression was quantified by qRT-PCR analysis. (A, middle) Decreased levels of miR-101, miR-26a, and miR-26b in NKYS upon MYC induction by tet-on. (A, right) MYC induction by tet-on increases EZH2 mRNA levels. (B, left) Depletion of MYC by siRNAs results in induction of miR-101, mir-26a, and miR-26b transcription in NKYS cells. Cells were transfected with MYC siRNA or nontargeting siRNA as a control. Cells were harvested 48 hours after transfection for mRNA analysis of miR-101 and miR-26 gene levels by real-time PCR. (B, right) ChIP-qPCR for endogenous MYC binding to miR-101, miR-26a, and miR-26b genes. Fold enrichment in the ChIP experiment represents the signal obtained after MYC immunoprecipitation followed by qPCR amplified by primer pairs that spanned gene promoters. (C, left) Correlation between MYC activation index and EZH2 mRNA levels. Cross: Normal tissue; Plus sign: Normal NK; Triangle: NKTL; Circle: Cell Lines. $R>0.95$, $P < 2.2*10^{-16}$. (C, right) Scatterplot showing the correlation between IHC MYC staining and EZH2 expression. Spearman correlation coefficient r for MYC v EZH2 = 0.76; $P < .0001$.

EZH2-positive samples have significantly higher EZH2 messenger RNA (mRNA) levels (Figure 1B). These data confirm that EZH2 is overexpressed in NKTL at both the mRNA and protein levels.

Loss of miR-26 and miR-101 contributes to the EZH2 upregulation in NKTL

Next, we sought to identify the mechanisms leading to EZH2 upregulation in NKTL. The genomic locus containing EZH2 is not commonly amplified in NKTL.[22] In our previous miRNA expression–profiling study, we found several miRNAs that were predicted to target EZH2 by various computational algorithms (supplemental Table 4) to be downregulated in NKTL.[19] Among these, the expression of miR-26a, miR-26b, and miR-101 has a significant inverse correlation with EZH2 when our previous GEP and miRNA profiling data were analyzed. miRNAs negatively regulate protein translation by predominantly destabilizing and, hence, decreasing their target mRNA levels.[23] In prostate, muscle, and B-cell lymphoma, miR-101, miR-26a, and miR-26b can negatively regulate EZH2 expression by binding to the highly conserved predicted binding sites within the 3′UTR of EZH2.[9,10] Using lentiviral transduction to express miR-101, miR-26a, and miR-26b in NKYS (supplemental Figure 2A, left), we observed that EZH2 expression was effectively attenuated (supplemental Figure 2A, right). These data suggest that EZH2 overexpression may be attributed to the deregulation of miR-101, miR-26a, and miR-26b in NK tumor cells.

MYC activation suppresses the expression of miR-26 and miR-101 in NKTL

As the genomic loci containing miR-101, miR-26a, and miR-26b are not recurrently deleted in the NKTL (data not shown), we looked for other mechanisms for their repression. On the basis of our previous study of gene expression in NKTL, which showed MYC activation,[4] and a recent paper showing that MYC activation can lead to repression of a many miRNAs in tumorigenesis,[24] we investigated whether MYC is involved in the suppression of miR-101 and miR-26 in malignant NK cells. When MYC expression was induced in NKYS cells using a tet-on system (Figure 2A, left), miR-101, miR-26a, and miR-26b was downregulated (Figure 2A, middle) with a corresponding (1.53-fold) increase in EZH2 mRNA (Figure 2A, right). Conversely, these 3 miRNAs were up-regulated by depletion of MYC using small interfering RNA (siRNA)–mediated knockdown (Figure 2B, left), and MYC depletion reduced EZH2 3′UTR luciferase reporter activity (supplemental

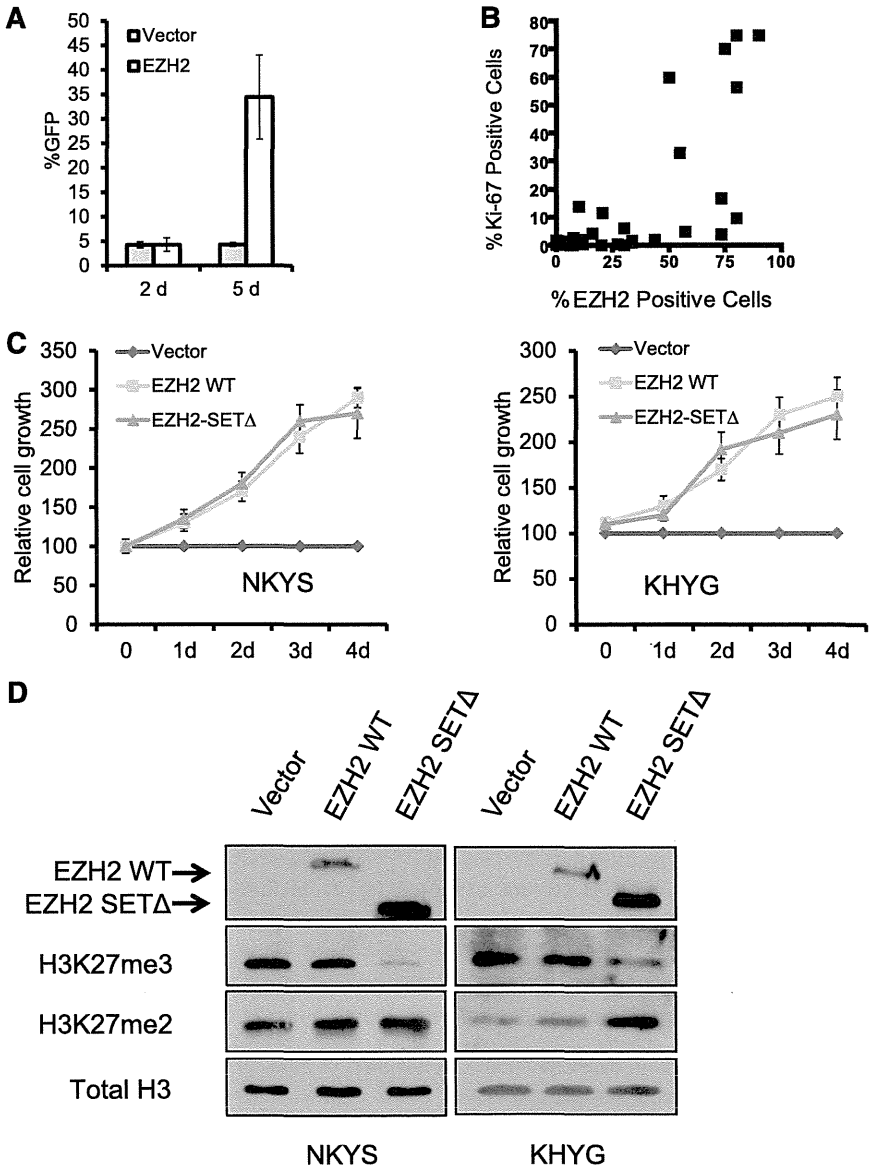

Figure 3. EZH2 overexpression in NKTL promotes cell growth independent of histone methyltransferase activity. (A) Primary NK cells transduced by EZH2 exhibit a growth advantage. Primary NK cells expressing ectopic EZH2 were monitored by a coexpressed GFP marker. Using our established viral infection protocol, we routinely obtained a transduction efficiency of 4.3% for normal NK cells. If EZH2 infection does not alter the cell growth, the EZH2-infected cell will not gain a growth advantage; thus, the percentage of GFP+ cells should remain at 4.3%. However, the percentage of GFP+ cells increased from approximately 4.3% at day 2 to ~34.4% at day 5, indicating an acquired growth advantage in these EZH2-infected cells. Antibiotic selection of positively infected cells was not done. (B) Scatterplot representation of the correlation between the percentage of Ki-67–positive cells and the percentage of EZH2-positive cells. Spearman correlation coefficient r for EZH2 v Ki67 = 0.73; $P < .0001$. (C) MTS proliferation assay showing that ectopic expression of EZH2 promotes cell growth of NKTL cell lines without requiring SET domain activity. Cells were cotransfected with pMAX-GFP and the control empty vector pcDNA4.1 or EZH2 expression plasmids. Cells transfected were subjected to proliferation assays for up to 96 hours. The cell growth (expressed as a percentage of the empty vector control) was determined by MTS assay as described in Materials and Methods. The mean values of triplicate samples are shown, and error bars indicate standard deviations. (D) Western blot analysis of EZH2, H3K27m3, and H3K27m2 in indicated samples. Expression of EZH2 WT and the SET-domain mutant was detected by the MYC-tag antibody. H3 was used as a loading control.

Figure 2B). However, this effect was still seen when the miR-101 and miR-26 binding sites in the EZH2 3′UTR were mutated, suggesting that other miRNAs or factors regulated by MYC may be involved. Furthermore, ChIP-quantitative polymerase chain reaction (qPCR) results revealed that MYC binds to the genomic locus of miR-26a and miR-26b (Figure 2B, right), consistent with previous reports.[24] Interestingly, it also revealed an association of MYC specifically with a conserved region upstream of miR-101 on chromosome 1 (Figure 2B, right). In summary, MYC activation suppresses the expression of miR-26a, miR-26b, and miR-101 in NKTL cell lines by direct binding to their genomic locus, and that MYC may stimulate EZH2 overexpression by repression of its negative regulatory miRNAs. Consistent with these in vitro findings, we observed a strong correlation between EZH2 transcript levels and MYC activation as measured by the gene expression–based MYC activation index[4] in our clinical GEP dataset (Figure 2C, left). In addition, there is also a positive correlation between the percentage of cells expressing EZH2 and nuclear MYC, which is a marker for MYC activation, detected by IHC analysis in NKTL tissue microarrays (Figure 2C, right). In addition, a significantly greater number of cells with nuclear MYC are detected in EZH2-positive samples (supplemental Figure 3A), suggesting that the data from NKTL cell lines are applicable to clinical samples.

EZH2 overexpression in NKTL confers a growth advantage independently of histone methyltransferase activity

Next, we investigated whether EZH2 is functionally important in NKTL. When EZH2 was introduced into primary NK cells purified from normal human peripheral blood, we observed an eightfold increase in the percentage of GFP(+) cells from day 2 to day 5 compared with vector control (Figure 3A), demonstrating that the overexpression of EZH2 is able to provide a growth advantage in normal primary human NK cells. We next analyzed the effect of increasing EZH2 on cell proliferation in NKTL cell lines. Ectopic expression of EZH2 through transient cotransfection with the GFP expression construct in NKYS cells for 3 days resulted in significantly higher percentage of viable GFP(+) cells in EZH2-transfected cells than in empty vector-transfected cells (supplemental Figure 4). This result suggests that EZH2 overexpression by transfection leads to

a competitive cell growth advantage. Consistent with these observations in the cell lines, a positive correlation between the expression of EZH2 and Ki-67, a marker of cell proliferation, was also observed in NKTL tumor samples (Figure 3B). Furthermore, EZH2 positivity is associated with a greater percentage of tumor cells expressing Ki-67 (supplemental Figure 3B).

Although EZH2 commonly exerts its oncogenic properties through H3K27 trimethylation (H3K27me3) and gene repression, we did not observe an association between EZH2 expression and the abundance of H3K27me3 by IHC studies in our clinical NKTL samples (supplemental Figure 3C). Interestingly, a lack of association between EZH2 and H3K27me3 has also been described in breast tumor subtypes[25,26] and in ovarian and pancreatic cancers.[26] This finding raises the possibility that EZH2 may have functions other than its activity on H3K27me3 in cancers, including NKTL. To investigate this possibility, we compared the ability of EZH2 wild-type (WT) and an EZH2 SET domain deletion mutant (EZH2 SETΔ) to increase the cell growth of NKTL cells. Interestingly, EZH2 SETΔ, which lacked the methyltransferase activity for H3K27me3, was still able to strongly promote cell growth of NKYS cells. This effect was as potent as EZH2 WT, as indicated by a similar increase in the percentage of GFP(+) cells with time (supplemental Figure 4), and increase in cell growth as measured by the MTS assay (Figure 3C). Both western blot (Figure 3D) and quantitative reverse-transcription PCR (qRT-PCR) analysis using a pair of primers that specifically amplifies the SET domain (supplemental Figure 5) confirmed the ectopic expression of EZH2 SETΔ in transfected cells. The ability of EZH2 SETΔ to deplete the H3K27me3 was also validated (Figure 3D; supplemental Figure 6C). These results indicate that the proproliferative property of EZH2 in NKTL is not mediated by its histone methyltransferase activity.

EZH2 directly activates CCND1 transcription by binding to its promoter independent of its methyltransferase activity in NKTL

To better understand how EZH2 promotes proliferation in NK cell lines, we explored the mechanism by which EZH2 regulates cell cycle genes. The study by Bracken and colleagues showed that suppression of EZH2 by RNA interference (RNAi) significantly decreased positive regulators of cell proliferation such as G1/*S*-cyclins,[27] so it is tempting to speculate that EZH2 directly regulates the transcription of these genes by binding to their genomic locus. The CCND1 transcript is reported to be upregulated in NKTL tissues compared with normal NK cells,[28] and high expression of CCND1 correlates with poor prognosis and decreased survival duration in NKTL.[29] Therefore, we examined whether the transcription of CCND1 is affected by EZH2 overexpression. Consistent with our findings on cell growth, qRT-PCR indicated that CCND1 mRNA levels increased substantially after EZH2 overexpression in NKYS (Figure 4A). Higher induction of CCND1 by EZH2-SETΔ could be explained by a previous study that ectopic EZH2 SETΔ depletes endogenous EZH2 and consistently displays higher levels of protein accumulation compared with the ectopic EZH2 WT.[30]

Next, we evaluated whether EZH2 can activate the activity of the CCND1 promoter in NKYS cells. Cotransfection of the EZH2 WT expression vector with the pGL4-CCND1-Luc reporter resulted in considerable activation of CCND1 promoter activity (Figure 4B). Consistent with prior results, activation of luciferase activity was also observed in cells transfected with EZH2 SETΔ (Figure 4B). Collectively, these results indicate that EZH2 positively regulates CCND1 transcription independent of its histone methyltransferase activity.

We then addressed whether EZH2 binds to the CCND1 promoter using ChIP-qPCR assays. Six pairs of primers, located sequentially along the proximal promoter, first exon, and intron 1 of CCND1 were used to quantify the ChIP-enriched DNA by real-time PCR (Figure 4C). A peak representing EZH2 binding was observed (~33-fold above background) at a region very close to the transcriptional start site of CCND1 (Figure 4D). ChIP using a control IgG showed no significant enrichment over the entire surveyed region (Figure 4D). By performing ChIP assays using a His-Tag antibody in NKYS transfected with His-Tagged EZH2 SETΔ, we showed that ectopically expressing EZH2 SETΔ resulted in significant enrichment of EZH2-DNA complexes, which was even higher than EZH2 WT (Figure 4E). This effect is specific to the SET domain, as EZH2 SANT domain deletion mutants abolished EZH2 transcriptional activity on the CCND1 promoter (Figure 4F). Furthermore, data from tumor samples that CCND1 mRNA levels correlate well with EZH2 mRNA levels are consistent with this finding (Figure 4G). Consistently, western blot analyses showed that CCND1 protein is expressed together with EZH2 in NK cell lines but not in normal NK cells (Figure 4H). Taken together, our findings identify CCND1 as a bona fide direct target of EZH2 in NKTL. Importantly, EZH2 acts as a transcriptional activator for the CCND1 gene without requiring histone methylation catalytic activity, which provides a mechanistic explanation for the proproliferative role of EZH2 SETΔ in NKTL.

Growth inhibition on depletion of endogenous EZH2 can be rescued by exogenous EZH2 SET mutants

Given that EZH2 is of functional importance in NKTL raises the possibility that targeting EZH2 may be a feasible strategy in NKTL. We first investigated the effects of depleting EZH2 on cell growth. Using 3 different short hairpin RNAs (shRNAs) targeting the EZH2 gene (Figure 5D; supplemental Figure 7A) in NKYS, we showed that depletion of EZH2 resulted in a substantial decrease in cell numbers, as revealed by the percentage of GFP+ cells (Figure 5A), and a specific concomitant decrease of CCND1 expression but not in other gene transcripts such as PRDM1 and IGF1 (Figure 5B; supplemental Figure 8). This result strengthens the postulation that EZH2 is required for expression of the proliferative gene CCND1 and suggests that downregulation of CCND1 is responsible for the reduction in cell growth in NKTL cells after EZH2 depletion.

Next, we sought to clarify if the reduction in cell growth is dependent on the methyltransferase activity of EZH2. Because EZH2 SETΔ is immune to EZH2 shRNA-2, which targets the SET domain, EZH2 shRNA-2 only depleted endogenous WT EZH2 but not the EZH2 SETΔ after being introduced into the cells, as expected (supplemental Figure 7B). Indeed, EZH2 SETΔ was able to prevent the reduction in cell numbers mediated by EZH2 shRNA-2, whereas reintroduction of EZH2 WT could not (Figure 5C, left). These rescue experiments excluded the possibility that the cell death phenotype occurred because of an off-target effect of EZH2 shRNA and, at the same time, confirming that the prosurvival effect of endogenous EZH2 does not require its enzymatic activity. Similar results were obtained in KHYG1 (Figure 5C, right), another NKTL cell line, indicating a consistent requirement for expression of EZH2 in the growth and survival of NK tumor cells.

Inhibition of EZH2 by 3-deazaneplanocin A (DZNep) induced growth inhibition and apoptosis of malignant NK cell lines

The effects seen with EZH2 knockdown suggest that EZH2 may be a therapeutic target in NKTL. We next explored the use of a

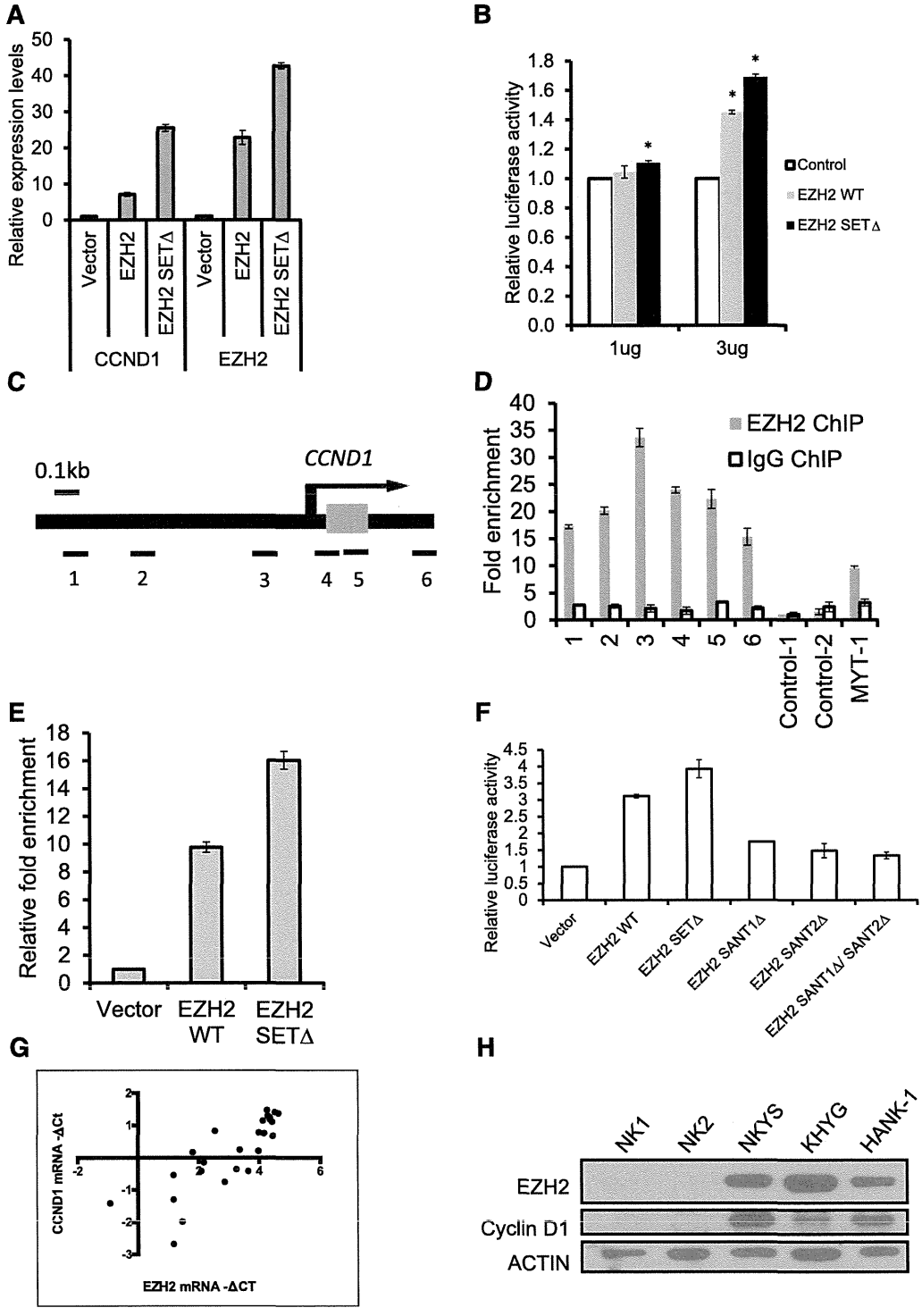

Figure 4. EZH2 positively regulates CCND1 transcription by binding to its promoter in NKTL cells. (A) Overexpression of EZH2 induces the expression of CCND1. Vectors expressing EZH2 (pcDNA-EZH2 or pcDNA-EZH2 SETΔ) were transiently transfected into NKYS cells. The RNA harvested from the cells at 24 hours after transfection was isolated, reverse-transcribed, subjected to qPCR by using primers specific for CCND1 mRNA, and normalized with GAPDH. (B) Luciferase promoter assay showing that EZH2 activates CCND1 transcription. NKYS cells were transfected with the luciferase reporter construct pGL4 containing the CCND1 promoter and various amounts of EZH2 WT/SETΔ plasmid or a control vector. Luciferase activities were measured after 24 hours. Luciferase readings were further normalized to the internal control pRL null. Results are presented as averages of triplicate experiments. Error bars represent standard deviation. * denotes $P < .01$ with respect to cells transfected with the same amount of control vector. (C) Genomic structure of human CCND1. The locations of the 6 pairs of primer sets used to detect the ChIP-enriched DNA fragments are indicated. (D) ChIP-qPCR for endogenous EZH2 binding to the CCND1 gene. ChIP assays were performed by using NKYS. Real-time PCR was performed with immunoprecipitated chromatin fragments obtained by using an anti-EZH2 antibody or an irrelevant antibody (IgG) as a control. A known EZH2 binding site in the promoter region of the MYT-1 gene was amplified as a positive control for the ChIP assays. (E) ChIP-qPCR for ectopically expressed EZH2 WT and EZH2 SETΔ binding to the CCND1 gene. ChIP assays were performed by using NKYS transfected by a pcDNA4.1/Myc-His vector or a plasmid expressing EZH2 WT and EZH2-SETΔ. Real-time PCR was performed with immunoprecipitated chromatin fragments obtained by using an anti-His antibody. Primer set 3, which amplifies a region representing EZH2 binding, was used to detect the ChIP-enriched DNA fragments. (F) Luciferase promoter assay showing the inability of EZH2 SANT domain deletion mutants to activate CCND1 transcription. NKYS were transfected with 3μg of EZH2 WT/SETΔ/SANTΔ plasmids or a control vector. Luciferase activities were measured after 24 hours. (G) Correlation between mRNA levels for EZH2 and CCND1 determined by qRT-PCR in NKTL clinical samples. Spearman correlation coefficient = 0.8608; $P < .0001$. (H) Western blot analysis of protein levels of CCND1 and EZH2 in NK cell lines and normal NK cells.

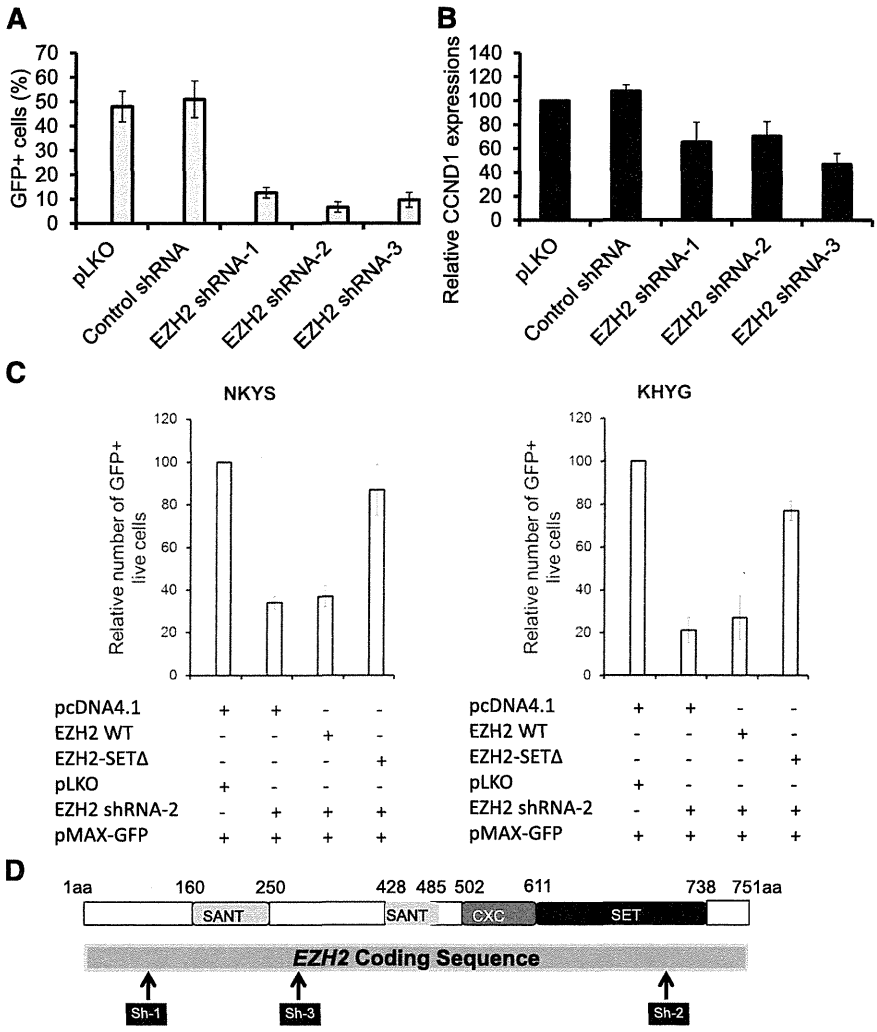

Figure 5. EZH2 depletion inhibits cell growth of NKTL tumor cells. (A) Effects of EZH2 knockdown on cell growth of NKYS cells. EZH2 shRNAs or control shRNA plasmids were cotransfected with a GFP-expressing plasmid pMAX-GFP in cells by electroporation. The percentage of GFP+ cells was determined by a Tali image-based cytometer at 18 hours after transfection. Cells transfected with EZH2 shRNA, but not those transfected with an empty vector or unrelated shRNA, exhibited a severe competitive growth disadvantage and cell death, as indicated by a significant depletion of GFP+ cells with time. (B) qRT-PCR analysis of CCND1 transcription in NKYS cells with EZH2 depleted by RNAi. (C) Rescue of EZH2 shRNA induced cell viability loss by forced expression of EZH2 SETΔ. Endogenous EZH2 was knocked down by an EZH2 shRNA-2, or was restored to physiological levels by ectopically expressing EZH2 shRNA2-resistant EZH2 SETΔ in NKYS and KHYG1 cells. Cells were cotransfected with EZH2 shRNA, together with either EZH2 WT or EZH2 SETΔ. Control transfections included a pLKO shRNA and pcDNA4.1, respectively. pMAX-GFP was cotransfected with other plasmids in each transfection to mark successfully transfected cells. The percentage of GFP+ live cells was determined by a Tali image-based cytometer at 18 hours after transfection. (D) Schematic description of EZH2 protein as well as the relative positions of regions targeted by EZH2 shRNAs. shRNAs expressed from a pLKO.1 vector targeting 3 regions of EZH2 are shown as black bars in relationship to the protein-coding regions.

compound capable of depleting PRC2 components called DZNep.[31] As reported previously,[31-34] DZNep effectively and dose-dependently reduced cellular levels of EZH2 in KHYG1 and NKYS, resulting in apoptosis as detected by PARP cleavage using western blot and Annexin V analysis by flow cytometry in a dose-dependent manner (Figure 6A,C). At the same time, CCND1 is down-regulated by DZNep at both the mRNA and protein levels (Figure 6A-B). In line with the diminished CCND1, NKYS treated with DZNep showed a substantial reduction in their proliferation rate, as illustrated by a 40% decrease in their BrdU incorporation (supplemental Figure 10). Thus, DZNep was able to phenocopy the effects of EZH2 knockdown on cell growth and CCND1 expression.

We next explored whether depletion of EZH2 is responsible for the cell growth inhibition and apoptosis observed by DZNep treatment in malignant NK cells. It is worth noting that DZNep depleted endogenous EZH2 protein but had no significant effect on exogenous EZH2 WT and EZH2 SETΔ (supplemental Figure 11). We observed a decrease in the DZNep-induced inhibition of cell growth in NKYS cells expressing both exogenous EZH2 WT and EZH2 SETΔ, compared with cells transfected with empty vector (Figure 6D). Although DZNep is not a specific inhibitor of EZH2 and may affect other molecules,[35] these findings indicate that DZNep-induced loss of cell viability in NKTL cells is, in large part, the result of a decrease in EZH2 levels.

Lastly, we evaluated the effects of DZNep on cell growth in other NK cell lines compared with normal NK cells. The MTS assay demonstrated that all of the additional 4 cell lines responded to DZNep treatment, whereas DZNep had minimal effects on normal NK cells (supplemental Figure 12A). Interestingly, the sensitivity of different cell lines to DZNep treatment seems to be related to EZH2 expression levels (supplemental Figure 12B).

Discussion

The data presented here show that EZH2 is aberrantly overexpressed in NKTL and that this is linked to Myc-mediated repression of miRNAs, such as miR26 and miR101 that normally target and inhibit EZH2 expression. This regulatory network demonstrated in NKTL further strengthens the recently proposed model that MYC may stimulate EZH2 overexpression by repression of its negative regulatory miRNAs.[9] Importantly, EZH2 overexpression is functionally important in NKTL, and the ability of EZH2 to promote proliferation in NKTL does not require its histone methyltransferase activity. Thus, for the first time our findings have uncovered a crucial and novel role for EZH2 in control of cell proliferation. Given our findings, it is likely that this unconventional role of EZH2

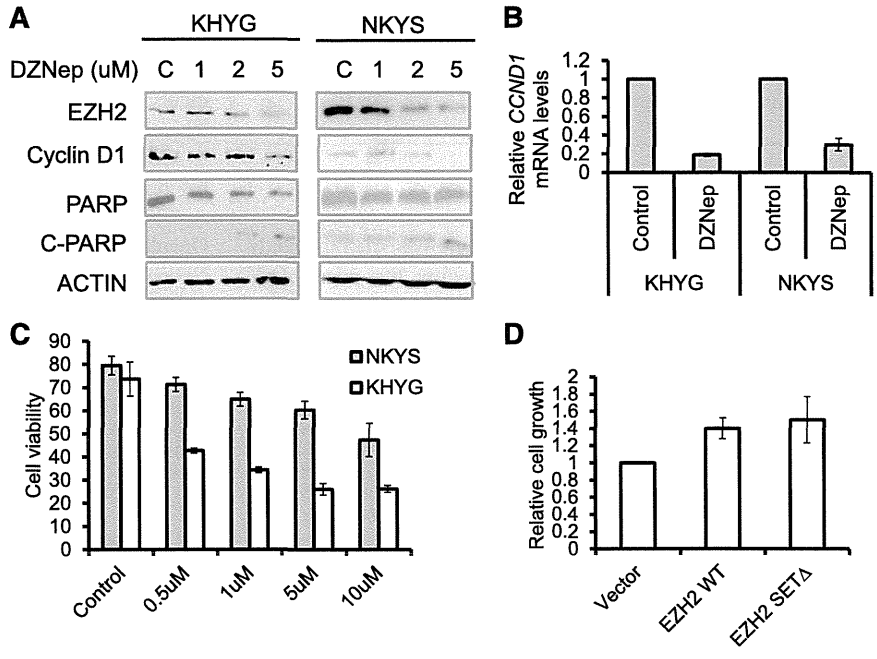

Figure 6. DZNep inhibits cell growth and induces apoptosis in NKTL tumor cells. (A) Western blot analysis of NK tumor cells exposed to increasing concentrations of DZNep showed a dose-dependent decrease in EZH2 protein, a decrease in CCND1 protein, and PARP cleavage in response to DZNep treatment. Cells were treated with indicated concentration of DZNep for 48 hours. Actin was used as a loading control. (B) Reduction of CCND1 mRNAs in DZNep-treated cells. The RNA harvested from the cells at 48 hours after treatment with DZNep at 5 μM, reverse-transcribed, subjected to qPCR by using primers specific for CCND1. (C) Quantification of cell viability in KHYG and NKYS cells treated with DZNep. Data are mean ±standard deviation of 3 independent experiments. (D) The rescued effects by EZH2 or EZH2Δ overexpression on DZNep-induced cell growth inhibition. Control plasmid or EZH2-expressing plasmids were cotransfected with pMAX-GFP to NKYS cells. Cells were then cultured in the absence or presence of DZNep at 10 μM for 48 hours. The percentage of GFP+ live cells was accessed by a Tali image-based cytometer.

seen in NTKL may represent a more general feature that may be also operational in other malignancies.

The best-understood mechanism by which EZH2 exerts its oncogenic function is to induce gene repression through its effect on chromatin via its histone methyltransferase activity that requires the SET domain of EZH2. However, there has been emerging evidence implying EZH2 functions that are not compatible with the transcription repression model. The oncogenic function of EZH2 has been attributed to the silencing of tumor suppressor genes such as *ARF*,[36] *p57KIP2*,[37] *FBXO32*,[38] *p27*,[33] and *BRCA1*.[39] Bracken and colleagues demonstrated that the downregulation of EZH2 expression by RNAi did not increase the expression of these negative regulators of the cell cycle.[27] On the other hand, there was a significant decrease in the positive regulators of cell proliferation such as G1/*S*-expressed cyclins in EZH2 knockdown cells.[27] These observations suggest that EZH2 is required for activation or maintenance of the activated state of certain genes in proliferating cells. The first evidence indicating a role of EZH2 in transcriptional activation was provided by Shi and colleagues[40] in which EZH2 interacts directly with estrogen receptor and β-catenin, functionally enhancing gene transactivation in the estrogen and Wnt pathways. In a more recent study, we demonstrated that EZH2 in aggressive breast cancer cells can positively modulate the NF-κB target gene by forming a ternary complex with RelA and RelB.[30] Notably, both studies demonstrated that this transcriptional activation activity is independent of the EZH2 SET domain and H3K27me3, although neither study has provided a phenotypic demonstration of such a histone methyltransferase–independent function of EZH2. Our results here clearly demonstrate that EZH2 enhances proliferation of malignant NK cells without requiring its enzyme activity, which highlights a mechanism not well recognized for EZH2 function.

Recent reports increasingly suggest an important role of EZH2 in a wide range of hematologic malignancies, yet its exact tumorigenic role and mechanism and the pathways it deregulates seem to vary in different malignancies. For example, we recently showed that EZH2 enzymatic function in acute myeloid leukemia is important and may be involved in deregulating metabolic pathway genes.[34] On the other hand, in the current study in NKTL, the nonenzymatic mechanism seems to be important in driving cell cycle progression by activating CCND1 expression. The understanding of how EZH2 works as an oncogene in different cancers has important therapeutic implications. EZH2 is currently thought to be important in oncogenesis through its enzymatic activity; hence, inhibitors in development are mostly targeting EZH2 enzymatic activity. Our study demonstrates that the oncogenic function of EZH2 may not always be dependent on its enzymatic activities. Therefore, small-molecule drugs that block EZH2 enzymatic activity will not work in these situations. This implies a need to review current therapeutic strategies. In view of the dual function of EZH2 in transcription activation and epigenetic repression, ideally there is a need to identify tumors where EZH2 is predominantly acting through its enzymatic function as a histone methyltransferase, inhibiting the protective role of tumor suppressor genes, as well as tumors where EZH2 is predominantly acting through activation of genes involved in other oncogenic pathways. This will ensure that the appropriate therapeutic strategy can be applied. Conversely, a compound that downregulates EZH2 protein may be effective in both scenarios. Therefore, therapeutic compounds that lead to EZH2 protein degradation rather than specific enzymatic inhibitors may be advantageous.

The proproliferative properties of EZH2 in NKTL support the rationale for using EZH2 inhibitors in the treatment of NKTL. Because targeting of EZH2 is an active area of drug development at present, there is great potential for the development of better treatment modalities. This is especially important for aggressive cancers, such as NKTL, for which no effective curative treatment is currently available.

Acknowledgments

The authors thank Prof. Daniel G. Tenen and Prof. H. Phillip Koeffler for their helpful suggestions.

W.-J.C. was supported by the National Medical Research Council Clinician Scientist Investigator Award. This work is supported in

part by the Singapore National Research Foundation and the Ministry of Education under the Research Center of Excellence Program to W.-J.C. S.-B.N. was supported by the National University Health System Clinician Scientist Program Award.

Authorship

Contribution: J.Y. and W.-J.C. conceived and designed the study, analyzed and interpreted the data, and wrote the paper; Q.Y. provided vital reagents and interpreted findings; S.-B.N. provided clinical samples, performed IHC scoring, interpreted the data, and wrote the paper; S.W. performed IHC scoring; J.Y., J.L.-S.T., B.L., T.L.K., J.T., V.S., S.-C.L., C.B., and S.-N.C. performed experiments; G.H. performed bioinformatics analysis; and N.S. contributed the cell lines.

Conflict-of-interest disclosure: The authors declare no competing financial interests.

Correspondence: Wee-Joo Chng, Department of Hematology-Oncology, National University Cancer Institute of Singapore, National University Health System, 1E, Kent Ridge Rd, Singapore 119228; e-mail: mdccwj@nus.edu.sg.

References

1. Lee J, Suh C, Park YH, et al. Extranodal natural killer T-cell lymphoma, nasal-type: a prognostic model from a retrospective multicenter study. *J Clin Oncol.* 2006;24(4):612-618.
2. Jaccard A, Hermine O. Extranodal natural killer/T-cell lymphoma: advances in the management. *Curr Opin Oncol.* 2011;23(5):429-435.
3. Gill H, Liang RH, Tse E. Extranodal natural-killer/t-cell lymphoma, nasal type. *Adv Hematol.* 2010; 2010:627401.
4. Ng SB, Selvarajan V, Huang G, et al. Activated oncogenic pathways and therapeutic targets in extranodal nasal-type NK/T cell lymphoma revealed by gene expression profiling. *J Pathol.* 2011;223(4):496-510.
5. Bracken AP, Dietrich N, Pasini D, Hansen KH, Helin K. Genome-wide mapping of Polycomb target genes unravels their roles in cell fate transitions. *Genes Dev.* 2006;20(9):1123-1136.
6. Chang CJ, Hung MC. The role of EZH2 in tumour progression. *Br J Cancer.* 2012;106(2):243-247.
7. Richter GH, Plehm S, Fasan A, et al. EZH2 is a mediator of EWS/FLI1 driven tumor growth and metastasis blocking endothelial and neuro-ectodermal differentiation. *Proc Natl Acad Sci USA.* 2009;106(13):5324-5329.
8. Chang CJ, Yang JY, Xia W, et al. EZH2 promotes expansion of breast tumor initiating cells through activation of RAF1-β-catenin signaling. *Cancer Cell.* 2011;19(1):86-100.
9. Sander S, Bullinger L, Klapproth K, et al. MYC stimulates EZH2 expression by repression of its negative regulator miR-26a. *Blood.* 2008;112(10): 4202-4212.
10. Varambally S, Cao Q, Mani RS, et al. Genomic loss of microRNA-101 leads to overexpression of histone methyltransferase EZH2 in cancer. *Science.* 2008;322(5908):1695-1699.
11. Cha TL, Zhou BP, Xia W, et al. Akt-mediated phosphorylation of EZH2 suppresses methylation of lysine 27 in histone H3. *Science.* 2005; 310(5746):306-310.
12. Wei Y, Chen YH, Li LY, et al. CDK1-dependent phosphorylation of EZH2 suppresses methylation of H3K27 and promotes osteogenic differentiation of human mesenchymal stem cells. *Nat Cell Biol.* 2011;13(1):87-94.
13. Morin RD, Johnson NA, Severson TM, et al. Somatic mutations altering EZH2 (Tyr641) in follicular and diffuse large B-cell lymphomas of germinal-center origin. *Nat Genet.* 2010;42(2): 181-185.
14. Yap DB, Chu J, Berg T, et al. Somatic mutations at EZH2 Y641 act dominantly through a mechanism of selectively altered PRC2 catalytic activity, to increase H3K27 trimethylation. *Blood.* 2011;117(8):2451-2459.
15. McCabe MT, Graves AP, Ganji G, et al. Mutation of A677 in histone methyltransferase EZH2 in human B-cell lymphoma promotes hypertrimethylation of histone H3 on lysine 27 (H3K27). *Proc Natl Acad Sci USA.* 2012;109(8): 2989-2994.
16. Nikoloski G, Langemeijer SM, Kuiper RP, et al. Somatic mutations of the histone methyltransferase gene EZH2 in myelodysplastic syndromes. *Nat Genet.* 2010;42(8):665-667.
17. Ernst T, Chase AJ, Score J, et al. Inactivating mutations of the histone methyltransferase gene EZH2 in myeloid disorders. *Nat Genet.* 2010; 42(8):722-726.
18. Ntziachristos P, Tsirigos A, Van Vlierberghe P, et al. Genetic inactivation of the polycomb repressive complex 2 in T cell acute lymphoblastic leukemia. *Nat Med.* 2012;18(2):298-301.
19. Ng SB, Yan J, Huang G, et al. Dysregulated microRNAs affect pathways and targets of biologic relevance in nasal-type natural killer/T-cell lymphoma. *Blood.* 2011;118(18):4919-4929.
20. Feng M, Li Z, Aau M, Wong CH, Yang X, Yu Q. Myc/miR-378/TOB2/cyclin D1 functional module regulates oncogenic transformation. *Oncogene.* 2011;30(19):2242-2251.
21. Chen X, Xu H, Yuan P, et al. Integration of external signaling pathways with the core transcriptional network in embryonic stem cells. *Cell.* 2008;133(6):1106-1117.
22. Iqbal J, Kucuk C, Deleeuw RJ, et al. Genomic analyses reveal global functional alterations that promote tumor growth and novel tumor suppressor genes in natural killer-cell malignancies. *Leukemia.* 2009;23(6):1139-1151.
23. Guo H, Ingolia NT, Weissman JS, Bartel DP. Mammalian microRNAs predominantly act to decrease target mRNA levels. *Nature.* 2010; 466(7308):835-840.
24. Chang TC, Yu D, Lee YS, et al. Widespread microRNA repression by Myc contributes to tumorigenesis. *Nat Genet.* 2008;40(1):43-50.
25. Holm K, Grabau D, Lövgren K, et al. Global H3K27 trimethylation and EZH2 abundance in breast tumor subtypes. *Mol Oncol.* 2012;6(5): 494-506.
26. Wei Y, Xia W, Zhang Z, et al. Loss of trimethylation at lysine 27 of histone H3 is a predictor of poor outcome in breast, ovarian, and pancreatic cancers. *Mol Carcinog.* 2008;47(9): 701-706.
27. Bracken AP, Pasini D, Capra M, Prosperini E, Colli E, Helin K. EZH2 is downstream of the pRB-E2F pathway, essential for proliferation and amplified in cancer. *EMBO J.* 2003;22(20): 5323-5335.
28. Huang Y, de Reyniès A, de Leval L, et al. Gene expression profiling identifies emerging oncogenic pathways operating in extranodal NK/T-cell lymphoma, nasal type. *Blood.* 2010;115(6): 1226-1237.
29. Cao W, Liu Y, Zhang H, et al. Expression of LMP-1 and Cyclin D1 protein is correlated with an unfavorable prognosis in nasal type NK/T cell lymphoma. *Mol Med Rep.* 2008;1(3):363-368.
30. Lee ST, Li Z, Wu Z, et al. Context-specific regulation of NF-κB target gene expression by EZH2 in breast cancers. *Mol Cell.* 2011;43(5): 798-810.
31. Tan J, Yang X, Zhuang L, et al. Pharmacologic disruption of Polycomb-repressive complex 2-mediated gene repression selectively induces apoptosis in cancer cells. *Genes Dev.* 2007;21(9): 1050-1063.
32. Xie Z, Bi C, Cheong LL, et al. Determinants of sensitivity to DZNep induced apoptosis in multiple myeloma cells. *PLoS ONE.* 2011;6(6):e21583.
33. Fiskus W, Wang Y, Sreekumar A, et al. Combined epigenetic therapy with the histone methyltransferase EZH2 inhibitor 3-deazaneplanocin A and the histone deacetylase inhibitor panobinostat against human AML cells. *Blood.* 2009;114(13):2733-2743.
34. Zhou J, Bi C, Cheong LL, et al. The histone methyltransferase inhibitor, DZNep, up-regulates TXNIP, increases ROS production, and targets leukemia cells in AML. *Blood.* 2011;118(10): 2830-2839.
35. Miranda TB, Cortez CC, Yoo CB, et al. DZNep is a global histone methylation inhibitor that reactivates developmental genes not silenced by DNA methylation. *Mol Cancer Ther.* 2009;8(6): 1579-1588.
36. Bracken AP, Kleine-Kohlbrecher D, Dietrich N, et al. The Polycomb group proteins bind throughout the INK4A-ARF locus and are disassociated in senescent cells. *Genes Dev.* 2007;21(5):525-530.
37. Yang X, Karuturi RK, Sun F, et al. CDKN1C (p57) is a direct target of EZH2 and suppressed by multiple epigenetic mechanisms in breast cancer cells. *PLoS ONE.* 2009;4(4):e5011.
38. Wu Z, Lee ST, Qiao Y, et al. Polycomb protein EZH2 regulates cancer cell fate decision in response to DNA damage. *Cell Death Differ.* 2011;18(11):1771-1779.
39. Gonzalez ME, Li X, Toy K, et al. Downregulation of EZH2 decreases growth of estrogen receptor-negative invasive breast carcinoma and requires BRCA1. *Oncogene.* 2009;28(6):843-853.
40. Shi B, Liang J, Yang X, et al. Integration of estrogen and Wnt signaling circuits by the polycomb group protein EZH2 in breast cancer cells. *Mol Cell Biol.* 2007;27(14):5105-5119.

Clinical Investigations

Respiration

Respiration
DOI: 10.1159/000355200

Received: May 18, 2013
Accepted after revision: August 19, 2013
Published online: December 7, 2013

Detection of Herpes Viruses by Multiplex and Real-Time Polymerase Chain Reaction in Bronchoalveolar Lavage Fluid of Patients with Acute Lung Injury or Acute Respiratory Distress Syndrome

Ryo Tachikawa[a] Keisuke Tomii[a] Ryutaro Seo[b] Kazuma Nagata[a] Kyoko Otsuka[a] Atsushi Nakagawa[a] Kojiro Otsuka[a] Hisako Hashimoto[c] Ken Watanabe[d] Norio Shimizu[d]

Departments of [a]Respiratory Medicine and [b]Critical Care, Kobe City Medical Center General Hospital, and [c]Department of Cell Therapy, Institute of Biomedical Research and Innovation, Kobe, and [d]Virology, Medical Research Institute, Tokyo Medical and Dental University, Tokyo, Japan

Key Words

Acute lung injury · Acute respiratory distress syndrome · Human herpes virus · Multiplex polymerase chain reaction · Real-time polymerase chain reaction

Abstract

Background: Human herpes viruses (HHVs) are important pathogens in acute lung injury (ALI) and acute respiratory distress syndrome (ARDS). Rapid and efficient diagnostic tools are needed to detect HHVs in the lung in ALI/ARDS patients. ***Objectives:*** This study aimed to evaluate the usefulness of multiplex and real-time polymerase chain reaction (PCR) analysis of bronchoalveolar lavage fluid (BALF) for detecting HHV reactivation in ALI/ARDS patients. ***Methods:*** Between August 2008 and July 2012, eighty-seven BALF samples were obtained from ALI/ARDS patients with unknown etiology and analyzed for HHVs. The types of HHVs in the BALF samples were determined using qualitative multiplex PCR followed by quantitative real-time PCR. ***Results:*** Multiplex PCR identified herpes simplex virus type 1 (HSV-1) (n = 11), Epstein-Barr virus (EBV) (n = 16), cytomegalovirus (CMV) (n = 21), HHV type 6 (HHV-6) (n = 2), and HHV-7 (n = 1) genomic DNA in 35 (40%) of the BALF samples, including 14 (16%) samples containing 2 or 3 HHV types. CMV and EBV reactivation was rare in immunocompetent patients, whereas reactivation of HSV-1 was predominantly observed in intubated patients regardless of their immune status. Overall, HHVs were almost exclusively found in patients with immunosuppression or endotracheal intubation. Real-time PCR detected 0.95–1.59 × 10^6 copies of viral DNA/μg human genome DNA, and HSV-1 (n = 4), CMV (n = 9), and HHV-6 (n = 1) were identified as potentially pathogenic agents. ***Conclusions:*** The implementation of multiplex and real-time PCR of BALF was feasible in ALI/ARDS patients, which allowed efficient detection and quantification of HHV DNA.

Introduction

Acute lung injury (ALI) and acute respiratory distress syndrome (ARDS) remain critical illnesses with substantial morbidity and mortality [1]. Despite advances in understanding the pathophysiology of ALI/ARDS, the

KARGER

E-Mail karger@karger.com
www.karger.com/res

0025–7931/13/0000–0000$38.00/0

Ryo Tachikawa, MD
Department of Respiratory Medicine
Kobe City Medical Center General Hospital
2-1-1, Minatojima-minamimachi, Chuo-ku, Kobe 650-0047 (Japan)
E-Mail ryotkw@gmail.com

mainstay of treatment for these diseases primarily involves supportive care and management of the underlying clinical disorder. Therefore, the pathogenic factors underlying these medical conditions need to be identified to indicate potential therapeutic interventions.

Human herpes viruses (HHVs) have been recognized as clinically important pathogens of pulmonary infections that can result in ALI/ARDS in immunocompromised patients [2–4], and they have also been recognized as potential pathogens in nonimmunocompromised critically ill patients [5–9]. However, there have been few comprehensive studies to date on the prevalence and pathogenic role of HHVs in ALI/ARDS patients, partly due to the limited diagnostic tools available for identifying different HHVs in a clinical sample.

In recent years, development of the multiplex polymerase chain reaction (PCR) assay has enabled simultaneous detection of a wide range of viruses [10]. Although a positive PCR for HHVs does not distinguish asymptomatic shedding from an active infection, quantification of the viral load in bronchoalveolar lavage fluid (BALF) could potentially differentiate between these two conditions [6, 11–13]. Therefore, rapid screening of BALF by qualitative multiplex PCR to identify virus-positive samples followed by quantitative PCR of the positive samples may be a useful diagnostic approach for evaluating lung diseases possibly caused by HHVs.

The aim of the present study was to evaluate the usefulness of multiplex and real-time PCR analysis of BALF for detecting HHV reactivation in ALI/ARDS patients.

Methods

Patients and Clinical Samples

Between August 2008 and July 2012, a total of 134 diagnostic bronchoalveolar lavage (BAL) procedures were performed in new-onset ALI/ARDS patients when the etiology of ALI/ARDS was unknown and was unlikely to be caused by bacterial pneumonia based on the clinical presentation, radiological findings, or the response to antibiotics. Of these, 87 BALF samples were analyzed for HHVs using multiplex PCR as part of the diagnostic examination, and the data were retrospectively examined in this study. BAL sampling was carried out via standard techniques, usually instilling five 30-ml aliquots of normal saline, and the specimens were stored at –80°C until the PCR was performed. The BALF was routinely tested for common pathogens (bacteria, fungi, and *Mycobacterium*) and for viral inclusion bodies by cytology. Additional microbiological studies, including quantitative PCR for *Pneumocyctis jirovecii* in BALF and cytomegalovirus (CMV) pp65 antigen levels in blood were performed as appropriate. Clinical and laboratory data were also collected from medical records. This study was approved by our institutional review board.

Classification of Viral Pneumonia Cases and Clinical Definitions

Classification of viral pneumonia cases was based on viral detection in BALF and on the following criteria: (1) proven viral pneumonia: specific cytopathic effects (inclusion bodies) in cells from BALF or transbronchial biopsy, (2) probable viral pneumonia: otherwise unexplained ALI/ARDS with a clinical response to specific antiviral agents, and (3) possible viral pneumonia: viral load $>10^4$ copies/μg DNA in BALF, otherwise unexplained ALI/ARDS, and antiviral agents ineffective or not administered. In possible viral pneumonia cases, there may be a clinical response to specific antiviral agents administered concurrently with efficacious treatments for known causes of ALI/ARDS. ALI/ARDS was defined according to previously reported criteria [14]. An immunocompromised patient was defined as one receiving immunosuppressants or corticosteroid therapy for more than 1 month or having AIDS.

PCR Analysis

HHV genomic DNA was measured by two independent PCR assays: qualitative multiplex PCR followed by quantitative real-time PCR of the HHV-positive samples detected by multiplex PCR.

The multiplex PCR was designed to identify the genomic DNA of 8 HHVs: herpes simplex virus type 1 (HSV-1), HSV-2, varicella zoster virus (VZV), Epstein-Barr virus (EBV), CMV, HHV type 6 (HHV-6), HHV-7, and HHV-8. DNA extraction was performed on 200- to 400-μl BALF samples using E21 virus minikits (Qiagen Inc., Valencia, Calif., USA). The multiplex PCR amplifications were set up in 2 capillaries (capillary 1: HSV-1, HSV-2, VZV, CMV, and HHV-6; capillary 2: EBV, HHV-7, and HHV-8), each containing 5 μl DNA extract, specific primers, hybridization probe mix, and Accuprime Taq (Invitrogen, Carlsbad, Calif., USA). The primers and probes for HHVs have been described previously [15] and are shown in table 1. The reactions were performed using the LightCycler PCR System (Roche, Switzerland) with the following conditions: an initial denaturation step at 95°C for 2 min, followed by 40 cycles at 95°C for 2 s, 58°C for 15 s, and 72°C for 15 s, with a final extension at 40°C for 30 s. Hybridization probes were then mixed with the PCR products and melting curves were analyzed using the LightCycler System. The sensitivity of the multiplex PCR analysis was 50 copies/tube.

Subsequently, for HHV-positive samples, real-time PCR was performed to measure the viral load using Amplitaq Gold and the Real-Time PCR 7300 System (ABI, Foster City, Calif., USA). The sequences of the primers and probes for the HHVs and the PCR conditions used in this study have been previously reported [16]. The BALF samples were also analyzed by PCR for the housekeeping gene glyceraldehyde-3-phosphate dehydrogenase (GAPDH) as an internal control, and the number of viral DNA copies was calculated as copies per microgram of human genome DNA. The viral DNA in the blood samples of selected patients was measured using the same multiplex PCR conditions, and the results were calculated as copies per milliliter of whole blood.

Statistics

Continuous variables are expressed as means ± SD unless stated otherwise. Categorical variables were compared using the χ^2 test or Fisher's exact test as appropriate. The CMV viral load in BALF was assessed as a diagnostic test for CMV pneumonia us-

Table 1. Sequences of primers and probes used in the multiplex PCR

Virus	Target gene	Primer sequence	Probe sequence
HSV-1, HSV-2[a]	polymerase	F: GCTCGAGTGCGAAAAAACGTTC R: TGCGGTTGATAAACGCGCAGT	3′FITC: GCGCACCAGATCCACGCCCTTGATGAGC LcRed604-5′: CTTGCCCCCGCAGATGACGCC
VZV	gene 29	F: TGTCCTAGAGGAGGTTTTATCTG R: CATCGTCTGTAAAGACTTAACCAG	3′FITC: GGGAAATCGAGAAACCACCCTATCCGAC LcRed640-5′: AAGTTCGCGGTATAATTGTCAGT
EBV	BamH1	F: CGCATAATGGCGGACCTAG R: CAAACAAGCCCACTCCCC	3′FITC: AAAGATAGCAGCAGCGCAGC LcRed640-5′: AACCATAGACCCGCTTCCTG
CMV	CMV glycoprotein	F: TACCCCTATCGCGTGTGTTC R: ATAGGAGGCGCCACGTATTC	3′FITC: TCGTCGTAGCTACGCTTACAT LcRed705-5′: ACACCACTTATCTGCTGGGCAGC
HHV-6	101k gene region	F: ACCCGAGAGATGATTTTGCG R: GCAGAAGACAGCAGCGAGTA	3′FITC: TAAGTAACCGTTTTCGTCCCA LcRed705-5′: GGGTCATTTATGTTATAGA
HHV-7	U57	F: GAAAAATCCGCCATAATAGC R: ATGGAACACCTATTAACGGC	3′FITC: GCCATAAGAAACAGGTACAGACATTGTCA LcRed705-5′: TTGTGAAATGTGTTGCG
HHV-8	EB BDLF1 ORF26	F: AGCCGAAAGGATTCCACCAT R: TCCGTGTTGTCTACGTCCAG	3′FITC: CCGGATGATGTAAATATGGCGGAAC LcRed705-5′: TGATCTATATACCACCAATGTGTCATTTATG

F = Forward primer; R = reverse primer.

[a] The primer sequences were the same for both HSV-1 and HSV-2, while the probe sequences were a complete match with the HSV-2 genome sequence but had a two-base mismatch with the HSV-1 genome sequence. Therefore, there was a difference in melting temperature between HSV-1 and HSV-2, enabling discrimination of these two viruses.

ing a receiver operating characteristic plot. $p < 0.05$ was considered statistically significant. All statistical analyses were performed using JMP 7.0.2 software (SAS Institute Inc., Cary, N.C., USA).

Results

Study Population

The clinical characteristics of the patients in this study are summarized in table 2. The underlying conditions were diverse and 49 (56%) patients were immunocompromised. ALI/ARDS developed in a nosocomial setting in 31 (35%) patients. Predominant ground-glass opacity mixed with focal air space consolidation was the most frequent radiological finding.

Viral Detection in BALF

The HHV virology results are summarized in table 3. Multiplex and real-time PCR detected HSV-1 in 11 (13%) BALF samples (2.92×10^2–6.22×10^5 copies/μg DNA), EBV in 16 (18%) samples (9.50×10^{-1}–6.62×10^4 copies/μg DNA), CMV in 21 (24%) samples (2.55–1.59×10^6 copies/μg DNA), HHV-6 in 2 (2%) samples (6.90×10^4–6.90×10^6 copies/μg DNA), and HHV-7 in 1 (1%) sample (3.12×10^3 copies/μg DNA). HSV-2, VZV, and HHV-8 were not detected. Overall, 35 (40%) patients were positive for at least one type of HHV, and multiple HHV types were detected in 14 (16%) patients.

The prevalence of HSV-1 was higher in intubated patients than in nonintubated patients (41 vs. 3%, $p < 0.0001$), but it was not significantly different between immunocompromised and immunocompetent patients (12 vs. 13%, $p = 0.90$) (fig. 1). In contrast, in CMV- and EBV-positive patients, the prevalence of CMV (fig. 2) and EBV (fig. 3) was not significantly different between intubated patients (31 and 18%, respectively) and nonintubated patients (22 and 18%, respectively) ($p = 0.33$ and $p = 1.00$, respectively), but it was significantly higher in immunocompromised patients (39 and 29%, respectively) than in immunocompetent patients (5 and 5%, respectively) ($p = 0.0003$ and $p = 0.006$, respectively). HHV-6- and HHV-7-positive BALF was obtained from immunocompromised patients. Overall, the prevalence of HHVs was higher in immunocompromised and/or intubated patients (55%; 32/58) than in immunocompetent patients without endotracheal intubation (10%; 3/29) ($p < 0.0001$).

Table 2. Baseline characteristics of the 87 patients in this study

Age, years	64.3±14.3
Male gender, n (%)	59 (68)
Underlying disease, n (%)	
Connective tissue disease	19 (22)
Posttransplant	9 (10)
Hematologic malignancy	8 (9)
Solid cancer	8 (9)
Postoperative	3 (3)
Hemodialysis	3 (3)
AIDS	2 (2)
Underlying pulmonary disease, n (%)	
IIP	21 (24)
CTD-IP	6 (7)
Immunocompromised, n (%)	49 (56)
Nosocomial onset, n (%)	31 (35)
Mechanical ventilation, n (%)	
At the time of BAL	27 (31)
Over the course of hospitalization	61 (70)
PaO_2/FIO_2, mm Hg	163±68.7
ALI, n (%)	28 (32)
ARDS, n (%)	59 (68)
Duration of symptoms, days	9.7±9.6
LDH, IU/l	543±363
CRP, mg/dl	10.3±3.3
CT findings (%)	
GGO only	12 (14)
GGO predominant	62 (71)
Consolidation predominant	13 (15)
BALF samples[a]	
Median total cell count (range), n × $10^5/mm^3$	2.35 (0.1–88.8)
Median neutrophils (range), %	28 (0–93)
Median lymphocytes (range), %	15 (1–82)
Median eosinophils (range), %	1 (0–46)
Median macrophages (range), %	32 (0–84)

IIP = Idiopathic interstitial pneumonia; CRP = C-reactive protein; LDH = lactate dehydrogenase; CTD-IP = connective tissue disease-associated interstitial pneumonia; GGO = ground-glass opacity.

[a] Fiberoptic bronchoscopy was performed with supplemental oxygen (n = 23), under noninvasive ventilation (n = 42), or under endotracheal intubation (n = 22).

Diagnosis

Fourteen patients in this study were diagnosed with viral pneumonia: 9 with CMV pneumonia (5 proven, 3 probable, 1 possible viral pneumonia), 4 with HSV-1 pneumonia (all possible viral pneumonia), and 1 with HHV-6 pneumonia (probable viral pneumonia) (table 4). Diagnoses of the other patients included acute exacerbation of interstitial pneumonia (n = 18), pneumocystis pneumonia (n = 13), other pulmonary infections (n = 7), diffuse alveolar hemorrhage (n = 7), septic ARDS (n = 3), drug-induced pneumonia (n = 3), other causes of ALI/ARDS (n = 11), and unidentified etiology (n = 12). HHVs were not detected in the BALF of patients with acute exacerbation of interstitial pneumonia, except in one BALF that had a low EBV viral load (278 copies/μg DNA). For a diagnosis of proven or probable CMV pneumonia, a cutoff value for the viral load in BALF of 1.39×10^4 copies/μg DNA had 87.5% sensitivity and 84.6% specificity.

Treatment and Outcome

Antiviral agents were administered to 13 patients with a diagnosis of viral pneumonia. Although respiratory improvement was seen, at least temporally, in 9 of the patients diagnosed with CMV or HHV-6 pneumonia, 10 (77%) patients eventually died due to a newly acquired infection, sustained respiratory failure, or multiorgan dysfunction (table 4). The overall in-hospital mortality in this cohort was 51%.

Discussion

This study showed that multiplex PCR and real-time PCR analysis of HHVs in BALF provided informative data regarding the epidemiologic characteristics of HHVs in ALI/ARDS patients with unknown etiology. To our knowledge, this is the first study to conduct comprehensive multiplex and real-time PCR analyses of HHVs in BALF of ALI/ARDS patients.

Viruses in the Herpesviridae family are the most common viral pathogens causing pulmonary infection in immunocompromised patients. Although CMV is best known for its propensity to cause pneumonia [2], other herpes viruses (e.g. HSV-1 [3, 17], VZV [18], EBV [19], and HHV-6 [20, 21]) have also been implicated as etiologic agents. Moreover, recent studies have documented frequent pulmonary reactivation and/or infection of HSV-1 [6, 7] and CMV [8, 9] in critically ill patients with no known immunocompromise. Therefore, ALI/ARDS patients with unknown etiology should be examined for possible viral pneumonia caused by HHVs, which often presents with bilateral ground-glass opacification and/or consolidation [17, 21, 22]. In this setting, the diagnosis must be broadened to a wide range of HHVs that can be efficiently examined by multiplex PCR instead of conventional microbiological tests for specific pathogens. In fact, this study found reactivation of 5 types of herpes viruses in 40% of ALI/ARDS patients, including 16% of patients with multiple types of HHVs in their BALF.

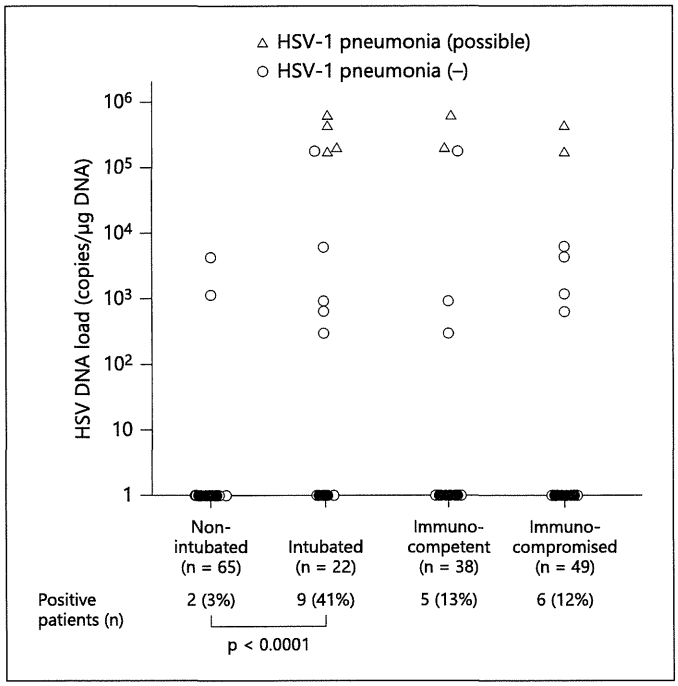

Fig. 1. HSV-1 prevalence and semi-log plot of the HSV-1 DNA load in BALF as a function of patient intubation or immune status. Negative PCR results were set to 1 ($\log_{10} 1 = 0$).

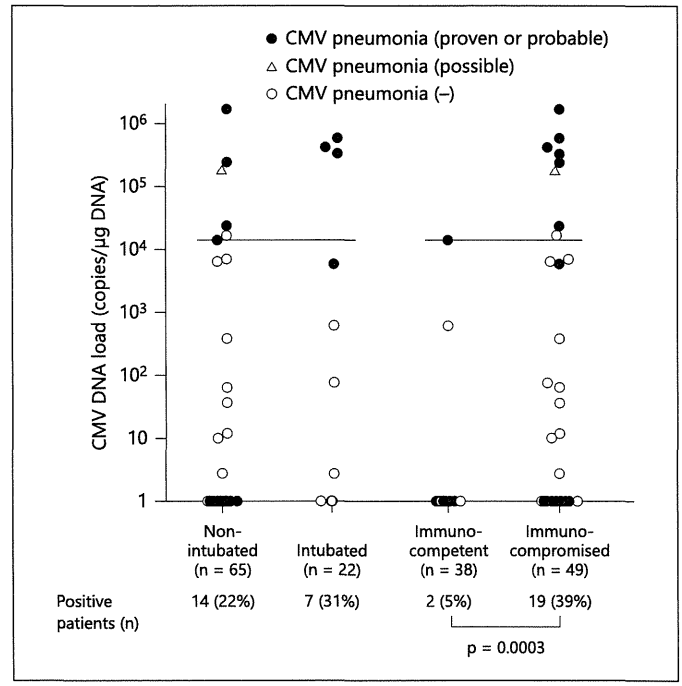

Fig. 2. CMV prevalence and semi-log plot of the CMV DNA load in BALF as a function of patient intubation or immune status. Negative PCR results were set to 1 ($\log_{10} 1 = 0$). The bar represents the cutoff value indicating CMV pneumonia (1.39×10^4 copies/μg DNA).

Table 3. HHV prevalence and viral load in BALF samples from the 87 patients in this study

	HSV-1	HSV-2	VZV	EBV	CMV	HHV-6	HHV-7	HHV-8
Positive BALF[a], n (%)	11 (13)	0	0	16 (18)	21 (24)	2 (2)	1 (1)	0
Viral load, copies/μg DNA	2.92×10^2–6.22×10^5	–	–	9.50×10^{-1}–6.62×10^4	2.55–1.59×10^6	6.90×10^4–6.90×10^6	3.12×10^3	–
BALF samples with a viral load, n								
≥0	0	–	–	2	3	0	0	–
≥10	0	–	–	2	4	0	0	–
$\geq10^2$	3	–	–	5	2	0	0	–
$\geq10^3$	3	–	–	3	3	0	1	–
$\geq10^4$	0	–	–	4	3	1	0	–
$\geq10^5$	5	–	–	0	5	0	0	–
$\geq10^6$	0	–	–	0	1	1	0	–

[a] Two types of HHVs were detected in 12 samples (EBV and CMV in 6, HSV-1 and EBV in 3, HSV-1 and CMV in 2, and CMV and HHV-6 in 1). Three types of HHVs were detected in 2 samples (EBV, CMV, and HHV-7 in 1 and HSV-1, EBV, and CMV in 1).

Considering the diversity of HHVs detected in this study, multiplex PCR has the additional advantage of being able to identify unexpected agents that might otherwise be overlooked, thereby enabling early therapeutic intervention.

This study provided insights into the epidemiologic features of herpes viruses in ALI/ARDS. Of note, reactivation of HSV-1 was predominantly observed in intubated patients regardless of their immune status, and a high HSV-1 DNA load in BALF was not associated with high-

Table 4. Laboratory and clinical findings of 14 patients diagnosed with or suspected of having viral pneumonia

Patient No.	Underlying disease	Virus	Diagnosis	DNA load		pp65 (+) cells	Other HHVs in BALF	Dominant CT finding	Antiviral agent	Outcome
				BAL copies/μg DNA	copies/ml blood					
1	SLE	CMV	proven	1.59×10^6	NA	82	none	GGO	ganciclovir	dead
2	posttransplant	CMV	proven	4.03×10^5	NA	206	EBV	GGO	ganciclovir	dead
3	SLE	CMV	proven	3.12×10^5	NA	34	EBV, HHV-7	GGO	ganciclovir	dead
4	MPA	CMV	proven	2.22×10^4	NA	0	none	GGO	ganciclovir	alive
5	DIHS	CMV	proven	1.39×10^4	NA	31	none	GGO	ganciclovir	dead
6	posttransplant	CMV	probable	5.65×10^5	NA	2	none	consolidation	ganciclovir	alive
7	SLE	CMV	probable	2.26×10^5	NA	30	none	GGO	ganciclovir	alive
8	DM-ILD	CMV	probable	5.70×10^3	NA	1	none	GGO	ganciclovir	dead
9	HIV-PCP	CMV	possible	1.70×10^5	NA	74	none	GGO	ganciclovir	alive
10	sepsis	HSV-1	possible	6.22×10^5	ND	NA	none	GGO	aciclovir	dead
11	posttransplant	HSV-1	possible	4.30×10^5	ND	0	none	GGO	none	dead
12	trauma	HSV-1	possible	2.00×10^5	NA	NA	none	GGO	aciclovir	dead
13	ML	HSV-1	possible	1.72×10^5	3.30×10^2	0	CMV	GGO	aciclovir	dead
14	posttransplant	HHV-6	probable	6.90×10^6	1.39×10^5	NA	none	GGO	foscarnet	dead

SLE = Systemic lupus erythematosus; MPA = microscopic polyangiitis; DIHS = drug-induced hypersensitivity syndrome; DM-ILD = dermatomyositis-associated interstitial lung disease; PCP = pneumocystis pneumonia; ML = malignant lymphoma; NA = not assessed; ND = not detected; GGO = ground-glass opacity.

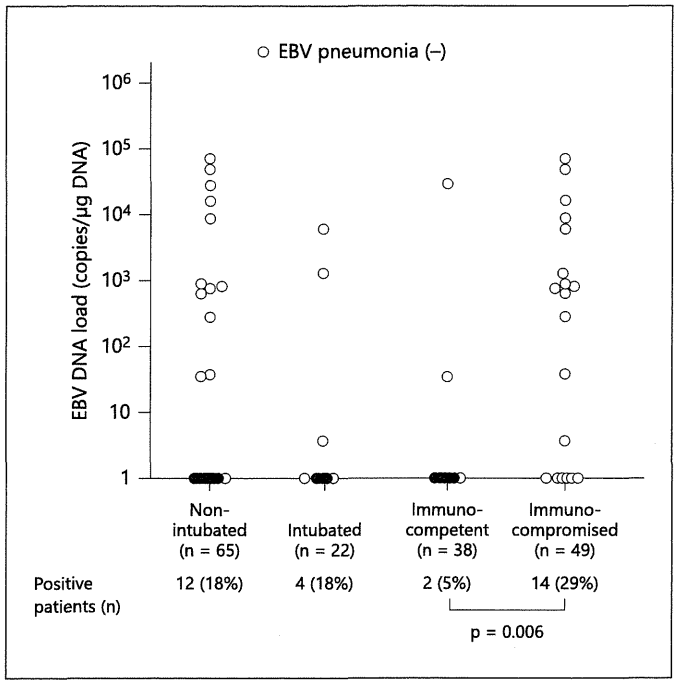

Fig. 3. EBV prevalence and semi-log plot of the EBV DNA load in BALF as a function of patient intubation or immune status. Negative PCR results were set to 1 ($\log_{10} 1 = 0$).

level viremia. These findings are in agreement with previous reports that HSV-1 pneumonia frequently presents as late-onset ventilator-associated pneumonia due to aspiration from the upper respiratory tract rather than pulmonary dissemination secondary to systemic viral infection [5, 6]. We also found that reactivation of HHVs other than HSV-1 mostly occurred in classically high-risk immunocompromised patients. Although recent studies have shown that CMV reactivation is common in nonimmunosuppressed, critically ill patients [8, 9], our results showed that CMV reactivation of the lung was rare in this patient population. Overall, clinically significant pulmonary reactivation of HHVs was almost exclusively observed in patients with endotracheal intubation or known immunocompromised status, indicating that patients with this clinical picture merit careful investigation for HHVs in the lung.

Viral pneumonia caused by HHVs still represents a diagnostic challenge. Demonstration of cytopathic effects by HHVs, indicating viral pathogenicity, is not a sensitive diagnostic tool and is often hard to obtain [23], while detection of HHVs via viral culture or PCR does not differentiate active infection from asymptomatic shedding. Therefore, combined use of real-time PCR with multiplex PCR is an integral part of the evaluation of HHV patho-